Stochastic Environmental Research and Risk Assessment
https://doi.org/10.1007/s00477-025-02961-x

ORIGINAL PAPER

Evolution of extreme precipitation in Spain: contribution of atmospheric dynamics and long-term trends

Santiago Beguería[1,2] · Miquel Tomas-Burguera[3] · Roberto Serrano-Notivoli[4] · David Barriopedro[5] · Sergio M. Vicente-Serrano[2,6]

Accepted: 12 March 2025

Abstract
The analysis of temporal changes in extreme event attributes, specifically magnitude and frequency, is hindered by the rarity and exceptional nature of the events being studied. The non-stationary extreme value theory (NSEVT) provides a well-established framework for assessing how extreme event probabilities vary as a function of one or more covariates. This study employs NSEVT to investigate the recent evolution and primary drivers of extreme precipitation in Spain, utilizing indices of three large-scale modes of atmospheric circulation and time as covariates. A non-stationary peaks-over-threshold model is applied to an observational network comprising 341 weather stations over the period 1951–2020. The results demonstrate that a multivariate model accounting for the influences of all covariates fits the data significantly better than simpler, univariate and stationary models in the majority of stations. The multivariate model effectively captures the spatial and temporal marginal influences of atmospheric dynamics on the magnitude-frequency relationship of different attributes of extreme precipitation events, including daily peak intensity and accumulated event precipitation. In contrast, the marginal influence of time is relatively small and sparse, lacking a spatially coherent pattern. Notably, the multivariate model reveals larger temporal influences than those inferred from the univariate model, with more stations displaying significant decreases than increases in extreme precipitation event attributes. These findings highlight the importance of considering multiple covariates and non-stationarity when analyzing temporal changes in extreme events.

Keywords Extreme precipitation · Trend analysis · Climate change · Non-stationary extreme value theory · Peaks over threshold · Atmospheric dynamics · Spain

1 Introduction

The extreme value theory (EVT) is the branch of statistics that deals with large deviations from the mean or the median values of a variable, including those that are larger than any previously observed. Pioneers of the EVT are the seminal works of Fréchet (1927), Fisher and Tippett (1928) and Gnedenko (1943), further codified by Weibull (1951) and Gumbel (1958). In climate science, the EVT provides tools for analysing the probabilities of extreme values of climatic variables, allowing for the construction of intensity-duration-frequency (IDF) curves and the computation of associated quantiles and return periods. Examples of the use of the EVT in climate science comprise analysis of the probability distributions of floods, extreme precipitation, heat and cold waves, sea waves, and tornados, among others (see references below).

✉ Santiago Beguería
santiago.begueria@csic.es

1 Estación Experimental de Aula Dei, Consejo Superior de Investigaciones Científicas (EEAD-CSIC), Zaragoza, Spain

2 Laboratorio de Clima y Servicios Climáticos (LCSC), Zaragoza, Spain

3 University of Illes Balears, Palma de Mallorca, Spain

4 Department of Geography and Regional Planning, Environmental Sciences Institute (IUCA), University of Zaragoza, Zaragoza, Spain

5 Instituto de Geociencias (IGEO), Consejo Superior de Investigaciones Científicas - Universidad Complutense de Madrid (CSIC - UCM), Madrid, Spain

6 Instituto Pirenaico de Ecología, Consejo Superior de Investigaciones Científicas (IPE-CSIC), Zaragoza, Spain

Published online: 28 March 2025

Extreme value analysis usually starts by sampling the highest observations of a time series. There are two classic approaches to do this: i) the *block maxima* (BM) approach, which involves taking the highest observations at fixed time intervals, such as the highest annual precipitation; and ii) the *peaks over threshold* (POT) approach, which considers all the observations over a pre-defined (sufficiently high) threshold (Leadbetter 1991). Despite the additional constraints involved in the POT approach (what constitutes a 'sufficiently high' threshold, and how to guarantee independence between two consecutive samples?), it has been favoured in practice over the BM one due to its capacity to better sample the distribution tail and to produce a larger sample since more than one event per time interval can be reatined. Each approach involves fitting the resulting sample to different probability distributions: the Extreme Value Distribution (or their particular cases: the Gumbel, Fréchet, and Weibull distributions), in the BM approach; or a combination of Poisson (to model the inter-arrival times) and Generalised Pareto (for magnitude) distributions, in the POT one (Balkema and De Haan 1974; Pickands 1975). Once the appropriate distribution is fitted, it is possible to derive useful statistics such as extreme quantiles or return periods, together with their uncertainty ranges.

Irrespective of the sampling method and the distributions involved, an important limitation of the classical EVT is the stationary assumption, i. e. that the distribution parameters remain constant. This is an important issue for assessing temporal trends in extremes, but also for exploring relationships between the distribution of extremes and other the covariates (e.g., atmospheric variables). In a climate change context the stationarity assumption is particularly questioned, and its violation might lead to biased estimation of quantiles and erroneous risk assessments (Yilmaz et al. 2014; Cheng and Aghakouchak 2014; Sarhadi et al. 2016; Ouarda et al. 2019).

In order to overcome this limitation some researchers used a split-sample approach where the data is divided into two or more sub-samples (for instance, two different 30-years periods) and independent models are fitted to each set and then compared (Li et al. 2005; Vicente-Serrano et al. 2009). A methodological refinement is the sliding-window approach, in which a fixed sampling window is moved over the data, for instance year by year (Hall and Tajvidi 2000; Fowler and Kilsby 2003; Beguería et al. 2011).

All these approaches are non-parametric, as independent models are fitted to each temporal sub-sample, and involve fitting a high number of parameters. The non-stationary extreme value theory (NSEVT), on the other hand, is an extension of the EVT that introduces parametric non-stationarity modelling of the distribution parameters (Coles et al. 2001). In the NSEVT the probability distribution coefficients can vary as a function of covariates (time or other), establishing a functional relationship between them. There are many different options to model this relationship, depending on the parameters (location, scale and shape) that are allowed to vary, and on the type of relationship (linear, logarithmic, etc.) established between them and the covariates.

Recent years have seen an increasing number of studies applying the NSEVT to climatic variables (e.g. Goswami et al. 2022; Hamdi et al. 2021; Tu and Yan 2021), helped by the development of new packages for the most popular programming and data analysis languages. By allowing the model parameters to change with time, the NSEVT allows undertaking studies to identify temporal trends in the occurrence of extreme events. One of the earliest examples used a non-stationary POT (NSPOT) approach to analyse trends in extreme ozone levels in Houston, Texas (Smith 1989). A very similar method was used to examine whether there was an increasing trend in the frequency of extreme daily precipitation in the USA over 1910-1996, finding evidence of an upward trend on 178 out of 183 stations (Smith 1999). Using a different approach for BM and POT sampling, Hall and Tajvidi (2000) analysed temporal variations in extreme wind storms in Sweden and extreme heat waves in Australia. Since then, there have been many application of the NSEVT to extreme event analysis. NSPOT approaches have been applied to assess the drivers of temperature extremes over the North Atlantic region (Nogaj et al. 2006) and France (Parey et al. 2007; Laurent and Parey 2007), river discharge in the Czech Republic (Yiou et al. 2006), and extreme wave heights in Washington (Méndez et al. 2006), while precipitation extreme drivers have been assessed in the UK (Maraun et al. 2010), France (Tramblay et al. 2012, 2013), Australia (Yilmaz et al. 2014; Yilmaz and Perera 2014), India Mondal and Mujumdar (2015); Agilan and Umamahesh (2015), China (Gao et al. 2016), South Korea (Lee et al. 2019), Canada (Thiombiano et al. 2017) and British Columbia (O'Brien and Burn 2018). As for the BM approach, non-stationary approaches were used to study the drivers of annual maxima precipitation in North Africa (Nasri et al. 2016), India (Ganguli and Coulibaly 2017; Agilan and Umamahesh 2017), Australia (Yilmaz et al. 2017), Ontario and California (Ouarda et al. 2019). These studies employed a wide diversity of covariates, depending on the region and purpose of the study. Typical covariates include large-scale circulation indices, but also other atmospheric (e.g. surface air temperature, moisture flux), oceanic (e.g. sea surface temperatures) and even socio-economic (e.g. urbanization) variables.

NSEVT methods have also been used to statistically downscale atmospheric model outputs and compute the expected probability of experiencing an extreme event.

Friederichs (2010) used a NSPOT model to derive probabilistic forecasts of extreme precipitation using covariates from a dynamic atmospheric model. Kallache et al. (2011) offers another example of a NSPOT approach to downscaling extreme precipitation from reanalysis and global circulation model output. NSPOT models have also been used to downscale future precipitation extremes from climate projections (Kyselỳ et al. 2010; Agilan and Umamahesh 2016; Roth et al. 2019).

For Spain, NSPOT models have only been applied to assess trends in hot extremes (Abaurrea et al. 2007) or precipitation extremes in specific regions (e.g. southwestern Spain, Acero et al. (2011)). Previous studies analysed trends in daily precipitation in Spain (Rodrigo 2010; Acero et al. 2011; Gallego et al. 2011; Serrano-Notivoli et al. 2018), and the influence of atmospheric dynamics on mean or heavy precipitation (Trigo et al. 2002; Queralt et al. 2009; Casanueva et al. 2014). However, to our knowledge there are no studies that considered together the influence of large-scale atmospheric modes of variability and temporal trends on extreme meteorological events. Based on the above-mentioned studies, daily precipitation trends in Spain exhibit large spatial and seasonal contrasts, but small changes (if any a slight decrease) in annual precipitation, and no clear trends in heavy precipitation, partially due to large internal variability and non-stationary influences of the major modes of atmospheric circulation in the region. These include the North Atlantic Oscillation (NAO) (Trigo et al. 2002; Queralt et al. 2009), and other atmospheric patterns such as the Mediterranean Oscillation (MO), the Western Mediterranean Oscillation (WEMO) or the East Atlantic pattern (Martin-Vide and Lopez-Bustins 2006; Ríos-Cornejo et al. 2015), which show non-stationary and spatially-varying influences on precipitation (Vicente-Serrano and López-Moreno 2008).

Here we present a NSPOT model to assess the combined influence of time and atmospheric circulation patterns on extreme precipitation. We apply this model to time series of extreme precipitation events using daily precipitation data from a station network on mainland Spain, for the period between 1951/01/01 and 2020/12/31. We analyse the performance of the non-stationary model, and describe the resulting spatial and temporal patterns of extreme precipitation. The results are compared to those obtained from a stationary model and univariate models with time or the circulation patterns as single covariates. The main objectives of the study are: 1) to asses the influence of atmospheric circulation patterns in the main precipitation events characteristics (intensity and magnitude), 2) to determine the existence of long-term trends, and 3) to investigate the interactions between the two factors (atmospheric circulation and trends).

2 Data and methods

2.1 Precipitation data

We compiled a data set consisting of 341 gap-free daily precipitation time series spanning the period 1951/01/01 and 2020/12/31 (70 years), using observational records provided by the Spanish meteorological agency (AEMET). The data set is evenly distributed across mainland Spain and the Balearic Islands (supplementary material, Figure A.1). It represents a subset of stations, which have been carefully selected from the complete AEMET network to ensure an adequate spatial coverage and temporal length.

As it is common in observational datasets, not all the raw series were complete. However, a majority of stations (75%) had less than 5% of missing data, and 25% of the series were almost complete (less than 1% of missing data). Only a small number of stations (n = 34) had gaps comprising more than 10% of the period, but they were still retained to ensure a good spatial coverage. Overall, only 5.1% of the data was missing.

To avoid introducing spurious effects in the analysis, a gap-filing procedure was used in order to get sequentially-complete series. To do that, the remaining daily precipitation series in the complete AEMET set (more than 10,000 stations) were used to fill-in the gaps. For each series in the main data set, a variable number of auxiliary series were selected based on their correlation with the main series and temporal coverage. The auxiliary series were selected if: i) they had a significantly large overlapping period (at least ten years) with the main series, allowing to reliably compute a correlation coefficient; and ii) they had data during the time periods when the main series had gaps.

The gap-filling procedure was based on the quantile-mapping method, consisting in the following steps:

1. Compute empirical cumulative distribution functions (ECDFs) of the main and auxiliary series over their overlapping period;
2. Transform the candidate and auxiliary series from their original units into quantiles, using the previously computed ECDFs;
3. For each gap, select the highest-correlated series with available data among the auxiliary series;
4. Assign the quantiles of the selected series to the missing values of the candidate series; and finally
5. Transform the quantiles of the candidate series back to the original precipitation units.

Unlike other methods such as regression which reduce the variance of the estimated data, one-to-one substitution has the least impact on the tails of the distribution. Furthermore,

quantile-mapping using the ECDFs eliminates possible bias between the auxiliary and the candidate series (Beguería et al. 2019). The gap-filling code is accessible at a public code repository (Beguería 2023).

2.2 Atmospheric circulation indices

Extreme precipitation events in Spain are influenced by various atmospheric circulation patterns, which vary in their importance along the year and spatially due to the country's diverse geography (Rodríguez-Puebla et al. 2001; Ramis et al. 2013; Pérez-Zanón et al. 2018). in winter, such events are commonly linked to low-pressure systems and cold fronts. In eastern Spain, convective processes driven by thermodynamic factors, particularly the Mediterranean Sea's temperature, also contribute to extreme precipitation, especially in spring and autumn (Ramis et al. 2013). Despite the complexity of these atmospheric conditions, certain atmospheric circulation indices effectively capture large-scale dynamics. The North Atlantic Oscillation, NAO (Stephenson et al. 2003), is a prime example, as it strongly influences precipitation patterns across parts of Spain, and plays a notable role in extreme events (Queralt et al. 2009; Vicente-Serrano et al. 2009). However, other mechanisms are also critical. The Western Mediterranean Oscillation, WEMO (Martin-Vide and Lopez-Bustins 2006), significantly impacts extreme precipitation along the Mediterranean coast, especially through its association with easterly flows (Lopez-Bustins et al. 2020; Vicente-Serrano et al. 2009). Similarly, the Mediterranean Oscillation, MO (Palutikof 2003), can greatly influence precipitation patterns, including extreme events, throughout Spain (Conte et al. 1989; Vicente-Serrano et al. 2009).

The NAO is the leading mode of variability of the North Atlantic. Based on the sea-level atmospheric pressure dipole between the Azores High and the Icelandic Low, its variability is linked to the North Atlantic storm track and westerly winds variability. The positive phase of the NAO is associated with enhanced westerlies and storm tracks affecting Europe's high latitudes, and high pressures over the Iberian Peninsula (IP). The opposite situation is found during the negative phase of the NAO, which promotes a southern shift of storm tracks, above-normal precipitation over large parts of the IP, and dry weather in northern and western Europe. The WEMO is a mode of variability of the Western Mediterranean, defined as the sea-level pressure difference between the Gibraltar Strait and the Adriatic Sea. During its positive phase high atmospheric pressures in Gibraltar with respect to the Adriatic promote north-westerly fluxes that enhance precipitation in the northern rim of the IP and decreases it in the Mediterranean region. During negative WEMO phases the pattern is reversed and precipitation over the Mediterranean is enhanced (Martín-Vide and López-Bustins, 2006). The MO, on the other hand, is a dipole between the west and east of the Mediterranean basin. During the positive phase of the MO, high pressures dominates over the Western Mediterranean, resulting in dry conditions over the IP. On the other hand, the presence of a low pressure system in Western Mediterranean leads to a negative phase of the MO, being more favorable to precipitation in the IP.

Although the main centres of these patterns are present throughout the entire year, their spatial patterns are usually stronger during winter, when they show a higher correlation with precipitation. During the summer, the atmospheric patterns weaken and in occasions are displaced, and their correlation with precipitation is lower due to the mainly convective origin of precipitation. Therefore, the influence of atmospheric circulation on extreme precipitation will be analysed here for the entire year, but also at the seasonal level.

For this study, daily time series of the three circulation modes were computed as standardised differences of sea-level pressure between pre-defined points: Reykjavik and Gibraltar for NAO; Gibraltar and Lod (Israel) for MO; and Gibraltar and Padova (Italy) for WEMO (Fig. 1). Sea level pressure data was obtained from the ERA5 reanalysis (Service 2017; Hersbach et al. 2020). The resulting time series are provided in the supplementary material (Figure A.2), aggregated at the monthly time scale to facilitate their visualisation. A twelve-month running average is also shown to highlight low-frequency variability and long-term trends.

This methodology has sometimes been criticised as possibly leading to a high correlation between the three indices due to sharing one of the two points of calculation (Gibraltar). Since time was also included in the analysis, it is also important to check for temporal trends in the time series of the indices. A simple correlation analysis shows that a positive correlation exists between MO and NAO (r = 0.318) and WEMO (r = 0.335), significant at the $\alpha = 0.05$ confidence level, while no significant correlation exists between NAO and WEMO (supplementary material, Figure A.3). Regarding temporal trends, there are significant correlations for NAO (r = 0.160) and WEMO (r = 0.126) with time, while MO showed no correlation. The possible effects of these correlations in the results will be discussed.

Before being used in the analysis, the circulation indices were transformed from the original standardised scale (z-scores) to a uniform distribution ranging between 0 and 1 (supplementary material, Figure A.4).

2.3 Stationary Peaks-Over-Threshold (POT) analysis

The Peaks-Over-Threshold (POT) approach is widely used in the analysis of extreme events, such as extreme

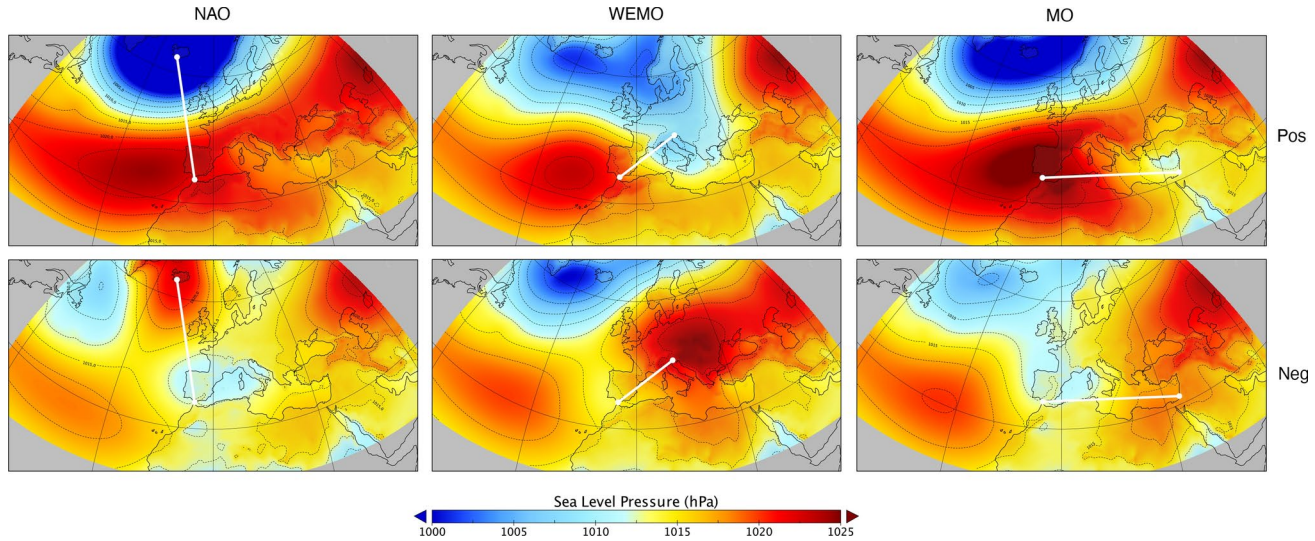

Fig. 1 Mean sea-level pressure fields (hPa) during positive (Pos) and negative (Neg) NAO, WEMO and MO, and grid cells used for computing the circulation indices

precipitation, to model values that exceed a high threshold. The POT approach relies on two key components: the Poisson process for modeling the occurrence of threshold exceedances, and the Generalized Pareto Distribution (GPD) for describing the magnitudes of these exceedances. In this context, the POT model can be used to assess return levels, which represent the magnitude of events expected to occur once on average within a given return period (e.g., the "100-year daily precipitation"). Below is an outline of the key steps and mathematical framework of the POT model (for a more thorough development, see Coles et al. (2001)).

The first step in the POT approach is selecting a sufficiently high threshold u. Values exceeding this threshold are considered "extreme events." The threshold u should be high enough to focus on the tail behaviour of the distribution, but not so high that there are too few exceedances for reliable statistical estimation.

The Poisson process is used to model the temporal frequency of exceedances over the threshold u. It assumes that exceedances occur randomly in time with a constant rate, denoted by λ, which is the rate of exceedances per unit of time. If $N(t)$ represents the number of exceedances within time period t, then $N(t)$ follows a Poisson distribution:

$$P(N(t) = k) = \frac{(\lambda t)^k e^{-\lambda t}}{k!}, \quad k = 0, 1, 2, \ldots \tag{1}$$

The Generalized Pareto Distribution (GPD) is used to model the magnitude of exceedances above the threshold u. If X is the observed precipitation, the exceedance $X - u$ (i.e., the difference between the observed value and the threshold) is modeled by the GPD. The probability density function (PDF) of the GPD for undefined $X > u$ is given by:

$$F(x|\sigma_u, \xi) = 1 - \left(1 + \xi \frac{x - u}{\sigma_u}\right)^{-1/\xi}, \quad x \geq u, \quad \xi \neq 0 \tag{2}$$

where σ_u is the scale parameter of the GPD, and ξ is the shape parameter.

σ controls the spread of the GPD, so larger values of σ lead to wider distributions, meaning the exceedances (values above the threshold) will be more dispersed and have larger variability. Conversely, smaller values of σ result in a more concentrated distribution, with exceedances being closer to the threshold and less variable.

ξ, on the other hand, describes the tail of the distribution, that is how rapidly the distribution decays and, therefore, how likely are extreme values far above the threshold. When ξ is positive the GPD has a heavy tail, meaning that extreme values far above the threshold are more likely. The distribution has infinite support, meaning there is no upper bound to how large values can be. When $\xi = 0$ the GPD reduces to the exponential distribution, which has a light tail, implying a lower likelihood of very extreme values compared to a heavy-tailed distribution. There is still no upper bound, but the probability of very large exceedances diminishes faster. When ξ is negative the GPD has a bounded upper tail, meaning there is a finite upper limit beyond which no values can occur. The distribution is truncated, and the maximum possible value of exceedances is given by $u - \sigma/\xi$. This can represent phenomena where extreme values are constrained by physical or natural limits.

Once the Poisson-GPD model is fitted to the data, it can be used to calculate return levels, which represent the magnitude of an event expected to occur once within a given return period. The return period T is the average time between events that exceed a certain magnitude, and

the return level x_T is the event magnitude associated with a return period T. The return period T is related to the rate of exceedances λ as follows:

$$T = \frac{1}{\lambda P(X > x_T | X > u)}$$

Using the GPD, the exceedance probability $P(X > x_T)$ can be expressed as:

$$P(X > x_T | X > u) = \left(1 + \xi \frac{x_T - u}{\sigma_u}\right)^{-1/\xi}$$

Solving for x_T, the return level corresponding to return period T, we get:

$$x_T = u + \frac{\sigma_u}{\xi}\left[(\lambda T)^{\xi} - 1\right], \quad \xi \neq 0 \tag{3}$$

Thus, the return level x_T represents the magnitude of precipitation that is expected to be exceeded once every T units of time.

2.4 Non-stationary Peaks-Over-Threshold (NSPOT) analysis

The POT approach is often applied under the assumption of stationarity, meaning that the parameters governing the P-GPD model are invariant. However, environmental systems and other processes often exhibit variability over time or in response to other covariates, necessitating an extension to the non-stationary POT model. In a non-stationary POT (NSPOT) approach, one or more parameters of the Poisson-GPD model are allowed to vary with time t or another covariate $Z(t)$. The parameters that can be allowed to vary include:

- Poisson process rate $\lambda(t)$, which governs the occurrence of extreme events.
- Threshold $u(t)$, which defines what constitutes an extreme event.
- GPD scale parameter $\sigma(t)$ and shape parameter $\xi(t)$, which describe the distribution of exceedance magnitudes.

One frequent formulation is to allow the Poisson rate $\lambda(t)$ to vary with time or covariates, while keeping the threshold u fixed. The Poisson rate, thus, becomes a function of time or a covariate:

$$\lambda(t) = f(Z(t)),$$

where $Z(t)$ is a time-varying covariate, such as the year, temperature, or a climatic index like the North Atlantic Oscillation (NAO). This approach allows for modelling the varying intensity of extreme event occurrences over time, reflecting changes in the frequency of extremes while assuming that the definition of "extreme" (i.e., the threshold) remains constant. Examples of this approach in the analysis of climate extremes include Yiou et al. (2006); Parey et al. (2007); Laurent and Parey (2007); Tramblay et al. (2013); Agilan and Umamahesh (2015); Silva et al. (2016).

An alternative approach is to keep the Poisson rate λ constant, while allowing the threshold $u(t)$ to vary over time or with a covariate:

$$u(t) = g(Z(t)),$$

where $g(Z(t))$ defines how the threshold changes in response to the covariate. This reflects the idea that the definition of an extreme event (the threshold) might change over time, while the overall occurrence rate of extreme events remains stable. Examples of this approach applied to climate extremes are Nogaj et al. (2006); Yiou et al. (2006); Parey et al. (2007); Laurent and Parey (2007); Tramblay et al. (2013); Agilan and Umamahesh (2015); Silva et al. (2016).

Both approaches provide flexible frameworks for modeling extremes in non-stationary systems and offer insights into how the occurrence or definition of extreme events may vary over time or in response to external drivers.

Most studies also include a non-stationary scale, as generally speaking a model with two (scale and either threshold or rate) parameters varying provide a better and more interpretable fit than models with only one varying parameter (Nogaj et al. 2006; Yilmaz et al. 2014; Thiombiano et al. 2017):

$$\sigma_u(t) = h(Z(t)).$$

Regarding the shape parameter, practice has shown that including a non-stationary ξ leads to highly uncertain and sometimes flawed estimates of the model's parameters (Friederichs 2010). Therefore, it is usually maintained stationary.

2.5 Implementation

2.5.1 Event sampling

A declustering process was applied to the daily precipitation time series prior to the analysis. The process consisted on grouping together series of consecutive wet days (days with precipitation higher than zero), to obtain so-called precipitation events. The reason to do that was twofold: on the one hand, to guarantee the independence of the events and

randomise the inter-arrival times, as required by the Poisson model; and on the other hand, to compute time series of event intensities (maximum daily intensity during the event) and event magnitudes (the sum of the daily precipitation values during the event).

From a hydrological perspective both the event's maximum intensities and magnitudes are relevant, since they often have distinct and important real-world impacts. Thus, while short and very intense events are often related to localised and immediate impacts such as flash floods, urban drainage and sewer overflows, damages to infrastructure and property, tree falls or landslides, long-lasting and cumulative precipitation events lead to slower-developed but more widespread hazards such as regional flooding and land sliding, groundwater flooding, agricultural loss, soil erosion or riverbank collapse. By treating event magnitudes as identically distributed variables, we captured the probabilistic nature of long-lasting extreme events without introducing unnecessary complexity from event duration.

In addition to precipitation variables, the mean values of the three circulation indices during each event were also computed (supplementary material, Figure A.5).

2.5.2 Threshold selection

For both event variables (intensity and magnitude), only the values above a sufficiently high threshold were retained for the analysis, therefore following a POT approach. The threshold was determined as the n-quantile of the precipitation events series intensity and magnitude.

The issue of threshold choice is complex, as it involves a necessary tradeoff between bias and variance. A lower threshold allows for a larger number of events, hence increasing the sample size and reducing the variance of the estimated parameters. Conversely, too low a threshold might violate the assumption of event independence, therefore introducing bias (Beguería 2005).

To address this issue, we used two complementary approaches. First, we applied the mean residual life (mean excess) plot, which helps identify a threshold beyond which the GPD assumption holds, indicated by an approximately linear relationship (Coles et al. 2001). Second, we checked the stability of the GPD model parameters at increasing values of the threshold. Additionally, we also checked tat the results were invariant to changes in the threshold.

2.5.3 Stationary and non-stationary models

After determining an appropriate threshold we fitted a stationary P-GPD model, which we termed M0, following Eqs. 1 and 2.

Then, we fit two alternative NSPOT models: a univariate non-stationary model M1, with threshold and scale parameters dependent on a single circulation index or time:

$$u(t) \;=\; u_0 + \beta Z(t); \quad \sigma_u(t) \;=\; \mathrm{e}^{\sigma_0 + \gamma Z(t)} \tag{4}$$

where u_0, β, σ_0, and γ) are regression coefficients, and $Z(t)$ is a covariate (totalling four models, one for each covariate); and a multi-variate model M2, with threshold and scale parameters dependent on time and the three circulation indices:

$$u(t) \;=\; u_0 + \boldsymbol{\beta} \mathrm{Z}(t); \quad \sigma_u(t) \;=\; \mathrm{e}^{\sigma_0 + \boldsymbol{\gamma} \mathrm{Z}(t)} \tag{5}$$

where Z is a vector of covariates and $(\boldsymbol{\beta}, \boldsymbol{\gamma})$ are vectors of coefficients. Notice the exponential link used for modelling the shape parameter, in order to ensure a positive value.

The Poisson rate parameter λ was determined directly by the mean annual frequency of events in the sample. Since we followed the second approach to the NSPOT model, this parameter was constant for all the model configurations. The relationship between the threshold and the covariates was modelled by the quantile regression method using the R package quantreg (Koenker 2022). Estimation of the GPD parameters, including the relationship between the scale parameter and the covariates, was performed using the maximum-likelihood (MLE) method as implemented in the R package ismev (Heffernan et al. 2018). MLE offered also estimations of the coefficients standard error, allowing for a significance test of each model parameter (t-test).

2.5.4 Model selection

likelihood ratio test is a common statistical tool used to assess whether allowing model parameters to vary over time or with covariates significantly improves model fit. The likelihood ratio test compares the likelihoods of the stationary and the non-stationary models. The test statistic is given by:

$$D \;=\; -2\left(\log L_1 - \log L_0\right),$$

where L_1 and L_0 are the likelihoods of the non-stationary and stationary models, respectively. The D statistic follows a chi-squared distribution χ^2_k with degrees of freedom equal to the difference between the lengths (parameter count) of the two models. A significant result suggests that the non-stationary model provides a better fit, indicating that time-varying or covariate-dependent parameters are warranted to capture trends or relationships in extreme events. Here, we used a significance level of $p < 0.05$.

Additionally, the Akaike Information Criterion (AIC) was used for comparing stationary and non-stationary POT

models, as well as different non-stationary models with different covariates (M1) or use univariate vs. multivariate frameworks (M1 vs M2). The AIC balances model fit with model complexity, penalising models with more parameters to prevent overfitting. It is calculated as:

$$\mathrm{AIC} = 2k - 2\log L$$

where k is the number of model parameters and L is the model's likelihood. A lower AIC value indicates a better tradeoff between fit and complexity. This approach is particularly useful when considering competing models, such as those with different time-varying parameters or covariate effects, as it helps identify the model that best balances explanatory power and simplicity.

3 Results

3.1 Analysis of a single station

We start presenting the results of the tested models for a particular station, 'Zaragoza Aula Dei (9499)', in North-East Spain (supplementary material Figure A.6). Located in the central Ebro River valley, this station is a good example as it is influenced by both Atlantic and Mediterranean influences. The results shown in this section correspond to the event's intensity, since the results for the event's magnitude are not much different.

The threshold u was established as the 90th percentile of the event's intensities. in addition to the stationary model (M0), four univariate non-stationary models (M1), one per each covariate, and one multivariate model (M2) were fitted to the dataset of exceedances above u. Table 1 provides AIC statistics of the different models, as well as the D test results comparing the non-stationary models against the stationary one. Maximum-likelihood estimated parameters and their standard errors are provided for the different model configurations in Table A.1.

Three non-stationary models provided a significantly better fit to the data than the stationary model: the univariate models (M1) with NAO or WEMO as covariates, and the multivariate model (M2) including all the covariables. Two non-stationary models were not significantly better than the stationary model: the univariate models (M1) with MO or time as covariates. The best model overall, according to the AIC statistic, was the multivariate model (M2).

Table 1 Model specification (covariates), values of the Akaike Information Criterion (AIC), and results of the D test (0 = negative; 1 = positive) for the univariate (M1) and multivariate (M2) non-stationary models as compared to the stationary model (M0), for precipitation intensity (mm day^{-1}) at the 'Zaragoza Aula Dei' (9499) station

Model	Covariate	AIC	D test
M0	–	2104	–
M1	NAO	2090	1
M1	WEMO	2016	1
M1	MO	2114	0
M1	Time	2129	0
M2	All	2008	1

Results of the stationary model (M0) are shown in Fig. 2. The mean excess plot is used as a graphic diagnostic for the POT threshold used to censor the data, and shows the mean excess for varying threshold values. The vertical line shows the 90th percentile of the data (u = 16 mm day^{-1}), which lead to a sample of n = 317 precipitation events (for λ = 4.53 events per year). The maximum likelihood GPD model coefficients were $\sigma = 9.862$ mm and $\xi = 0.0238$, with standard errors 0.816 and 0.0608, respectively. The value of ξ slightly higher than zero suggested a heavy tail. However, the probability of $\xi \leq 0$ was 0.348, so the possibility of the shape parameter not being positive could not be ruled out.

The return level plot provides the precipitation intensity as a function of the expected return period. As a reference, it also shows empirically-estimated return periods for the precipitation events above the threshold, although it must we warned that the method does not aim at fitting the empirical quantiles directly.

Figure 2 also includes two goodness of fit plots, in the form of probability-probability and quantile-quantile plots. Both plots show a satisfactory alignment of the points along the 1:1 line, indicating a good fit of the model to the empirical observations.

The selection of the threshold for the Peaks-Over-Threshold (POT) analysis is a critical aspect of the methodology, as detailed in the previous section. Given the inherent subjectivity in this choice, we conducted a robustness check to ensure that the 90th percentile was sufficiently high for the Poisson-Generalized Pareto (P-GP) model assumptions to hold. Specifically, we examined the stability of the maximum likelihood estimates for the shape parameter ξ and modified scale parameter ($\sigma' = \sigma - \xi * u$) across a range of thresholds u from the 85th to the 99th percentile (Fig. 3, Table A.3). As expected for a well-fitting GPD model, these parameters remained largely stable as u increased, confirming that the 90th percentile was an appropriate threshold. Moreover, return level plots using thresholds above the 85th percentile showed no significant differences, aside from natural random variability (Figure A.7) To provide further context, the estimated 100-year return levels with models for thresholds at the 85th, 90th, and 95th percentiles were 79.7 (7.96), 80.9 (9.55), and 76.5 (7.13) mm day^{-1}, respectively, indicating consistency in extreme event estimation across different thresholds.

Figure 4 illustrates the M1 model with WEMO as a covariate, which got the lowest AIC statistic (2016) among

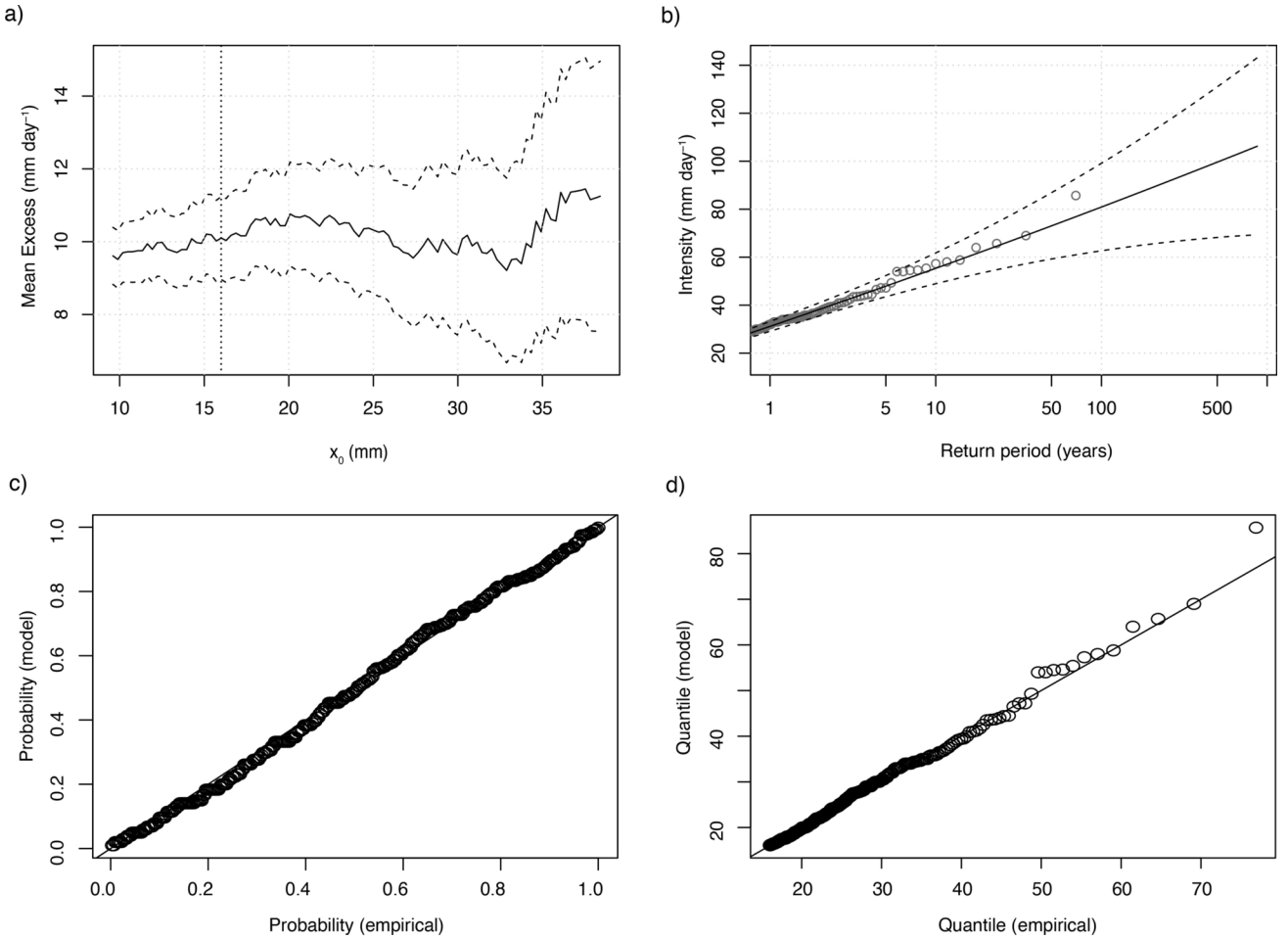

Fig. 2 Stationary extreme value analysis of precipitation intensity (mm day^{-1}) at 'Zaragoza Aula Dei' (9499) station: mean residual life plot (mean excess over threshold u, and approximate 95% confidence intervals), with indication of the 90th quantile (vertical line) (**a**); return level plot relating event's intensity and its expected mean return period (solid line), with 95% confidence bands (dashed lines), and empirical quantiles of observed events (circles) (**b**); probability-probability plot (**c**) and quantile-quantile plot (**d**) of modelled vs. empirical event probabilities

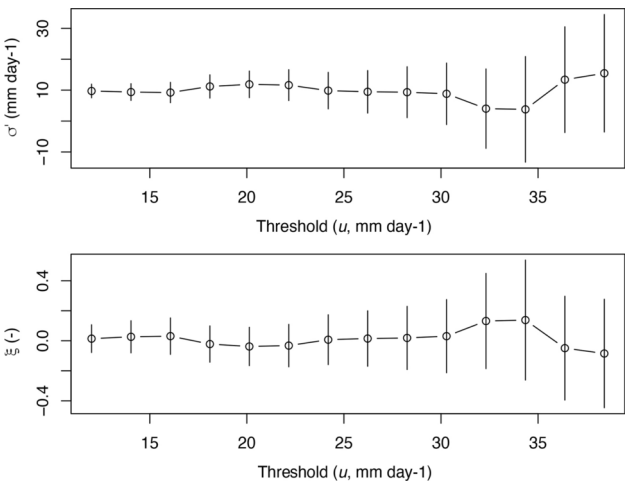

Fig. 3 Maximum likelihood estimates and confidence intervals of the shape (ξ) and modified scale (σ') parameters over a range of thresholds spanning between the 85th and the 99th quantiles of the event's intensity at 'Zaragoza Aula Dei' (9499) station

the three circulation indices. The first two plots (**a**, **b**) show the functional relationship between the threshold (u) and scale (σ) parameters and the WEMO index. There is a clear relationship between extreme precipitation and WEMO, since the most extreme events tended to coincide with low (negative) values of WEMO, while the highest events recorded during high (positive) WEMO were much lower in comparison. As a result, there is a decreasing relationship of u with WEMO. σ also exhibits substantial variation as a function of WEMO, with values more than two times higher for negative than for positive WEMO. As a result, the frequency-magnitude relationship changes noticeably as a function of WEMO (return plots in **c**, **d**). In contrast with model M0 (Fig. 2), the return level plot (**c**) now includes several lines (isohyets), corresponding to different values of WEMO. As an alternate option, plot (**d**) shows return level isolines as a function of both WEMO and return period. Differences for the 10-year return period event, for instance,

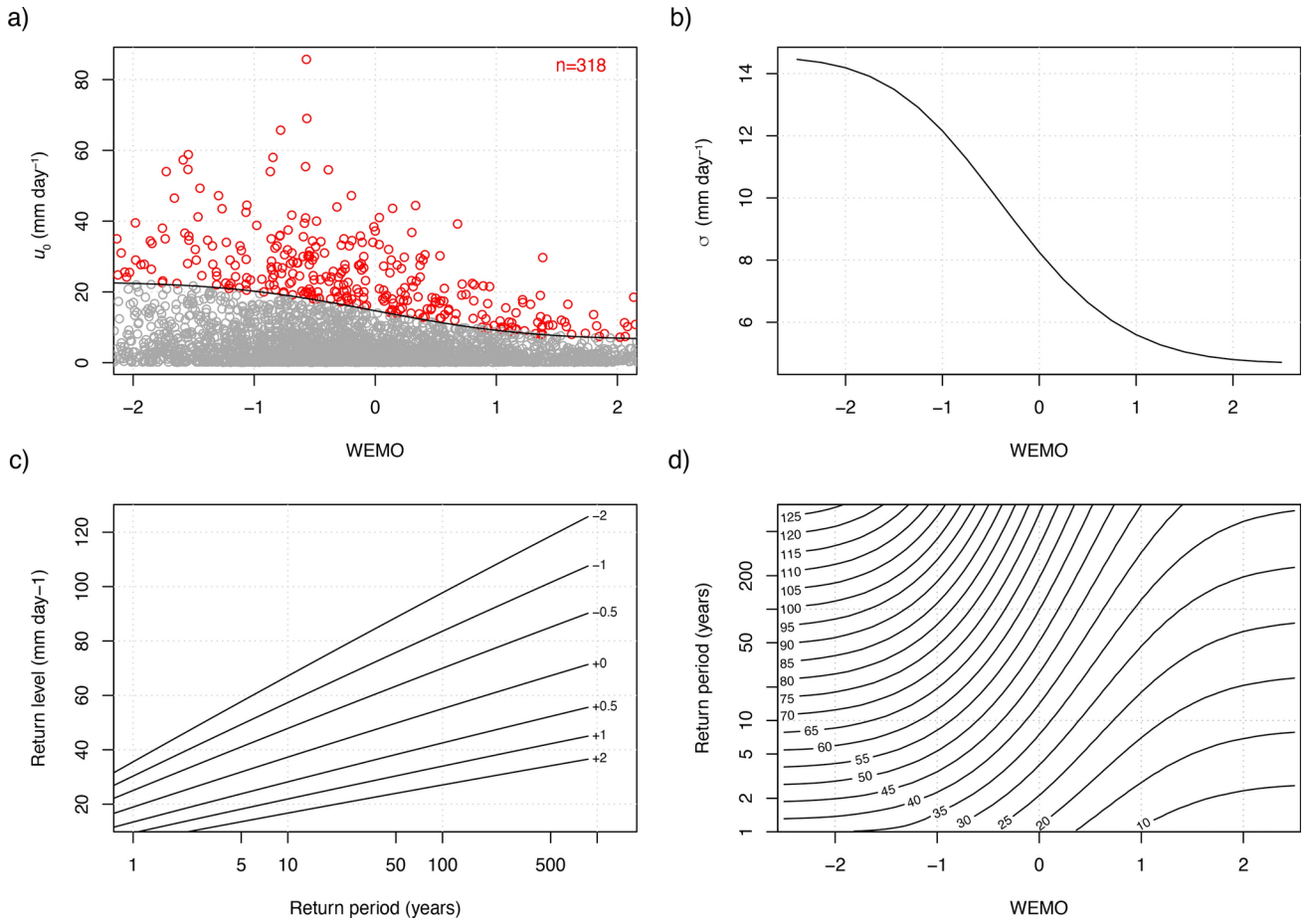

Fig. 4 Non-stationary univariate extreme value analysis of precipitation event intensity at 'Zaragoza Aula Dei' (9499) station: threshold (**a**) and scale (**b**) parameter models as a function of the WEMO index, with red circles denoting the observed events above the threshold; return level plot for different values of WEMO (**c**); contour plot of return levels (mm day^{-1}) as a function of the WEMO index (**d**)

are as high as 70 mm day^{-1} for WEMO = -2, vs. 17 mm day^{-1} for WEMO = 2. This difference can also be detected following different isohyets. Thus, while 30 mm day^{-1} corresponds to a return period of less than one year in one extreme of the WEMO range, it achieves a return period of 100 years in the other extreme.

Results of model M1 with time as covariate offer an insight on possible temporal trends in extreme precipitation intensity. This model, unlike the previous one, was not significantly better than M0 according to the D test, and yielded a higher AIC value. Despite this, the model shows a weak decreasing relationship of the two non-stationary model parameters with time (Fig. 5). The return level plots show lower expected events at the end of the study period (t = 70, corresponding to year 2020) than at the beginning (t = 1, year 1951). For instance, the 10-year return period event varied between 62 and 48 mm day^{-1}. That is, the model suggests a (non-significant) decreasing trend in extreme precipitation intensity at this station.

Figure 6 provides bi-variate return level plots for the M2 model, including the three circulation indices and time as covariates. Bi-variate plots for the two non-stationary parameters (u and σ) are provided as supplementary material (Figures A.8 and A.9). M2 was the best performing model at this station, according to the AIC statistic. It is interesting to assess the changes in the marginal relationships with the covariates, that is once the other covariates have also been considered. As expected, the most extreme events are conditioned to negative values of both WEMO and NAO, with a less pronounced effect of MO than seen in model M1. In the case of time, it shows a slightly decreasing trend once the variability of the three circulation indices is accounted for, but this effect is even smaller than in model M1. According to the t-test, the three coefficients for the circulation indices achieved significance, while the time coefficient was not significantly different from zero. Therefore, there is no evidence of a significant long-term change in extreme precipitation intensity at this station.

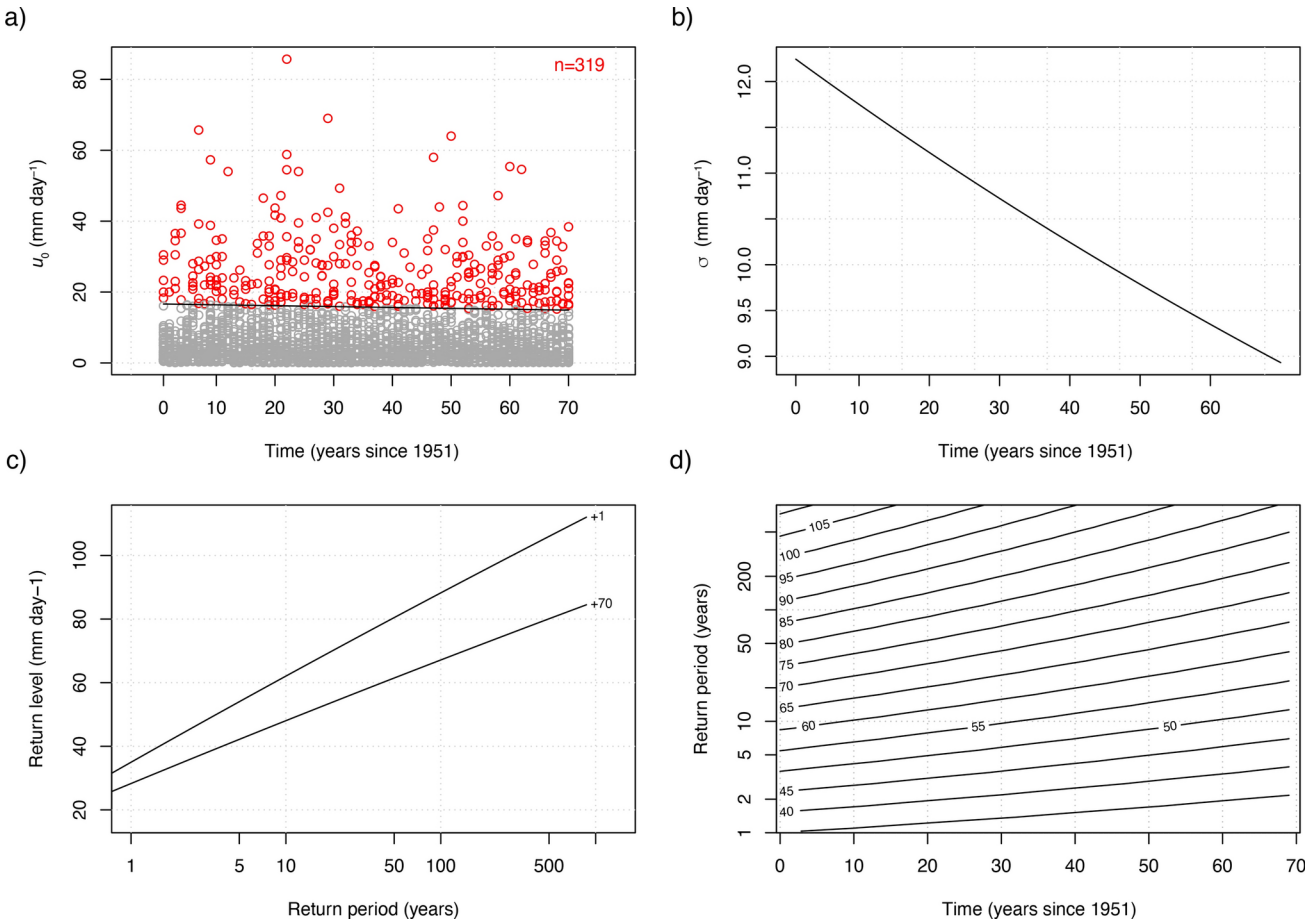

Fig. 5 Non-stationary univariate extreme value analysis of precipitation event intensity at 'Zaragoza Aula Dei' (9499) station: threshold (**a**) and scale (**b**) parameter models as a function of time (years since 1951/01/01), with red circles denoting the observed events above the threshold; return level plot for different times, with t = 1 corresponding to year 1951 and t = 70 to 2020 (**c**); contour plot of return levels (mm day^{-1}) as a function of time (**d**)

3.2 Whole network analysis: stationary model

Results of the stationary model applied to the whole station network allows assessing for spatial differences in the main characteristics of extreme precipitation events over the study area. The spatial distribution of the expected 100-year event shows interesting differences between the event's intensity and magnitude (Fig. 7). The highest intensities are found along the Mediterranean coast and in the Balearic Islands, with values in excess of 300 mm day^{-1}, reflecting the convective nature of high precipitation events over the Mediterranean façade of the IP. The lowest expected intensities, amounting around 50 mm day^{-1}, are found in the centre of the IP and the high valleys of the Duero and Tajo Rivers. The values increase towards the west and the north along the Atlantic coast, where they reach 100-200 mm day^{-1}.

In the case of the event's magnitude, the highest values are found again in the Mediterranean coast, but also over a large area under the Atlantic influence (North, West and South-West). In some of these areas, cumulative precipitation in excess of 800 mm can be expected during a single precipitation event, which may last for several days. Towards the interior of the IP the magnitudes rapidly decrease to less than 200 mm.

At the seasonal scale, the spatial patterns do not vary substantially with respect to the annual scale, but there are differences in the intensity and magnitude of the expected events (supplementary material, Figure A.12). Thus, the highest events are expected in autumn and winter, followed by spring and then summer. These results are in agreement with the contrasting characteristics (precipitation regime, seasonality and time-scale) of the weather systems responsible for causing high precipitation events across the territory: synoptic long-lasting winter fronts and extratropical cyclones of moderate intensity in western and northern Spain, and mesoscale short-lived intense convective systems in the Mediterranean, which are common in autumn (García-Herrera et al. 2005).

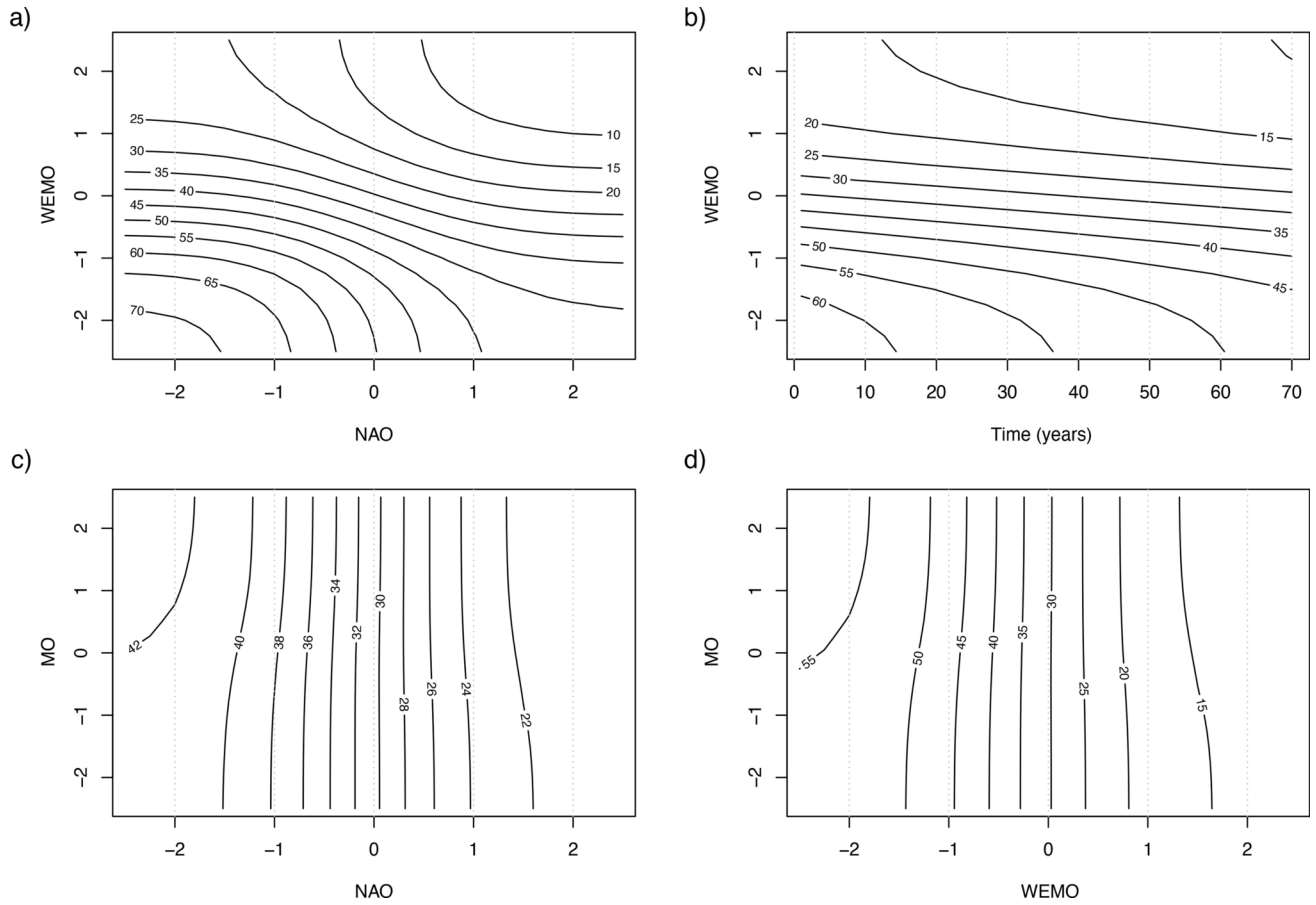

Fig. 6 Non-stationary multivariate extreme value analysis of precipitation event intensity at 'Zaragoza Aula Dei' (9499) station: bi-variate return level plots, with maximum expected intensity (mm day^{-1}) in contours

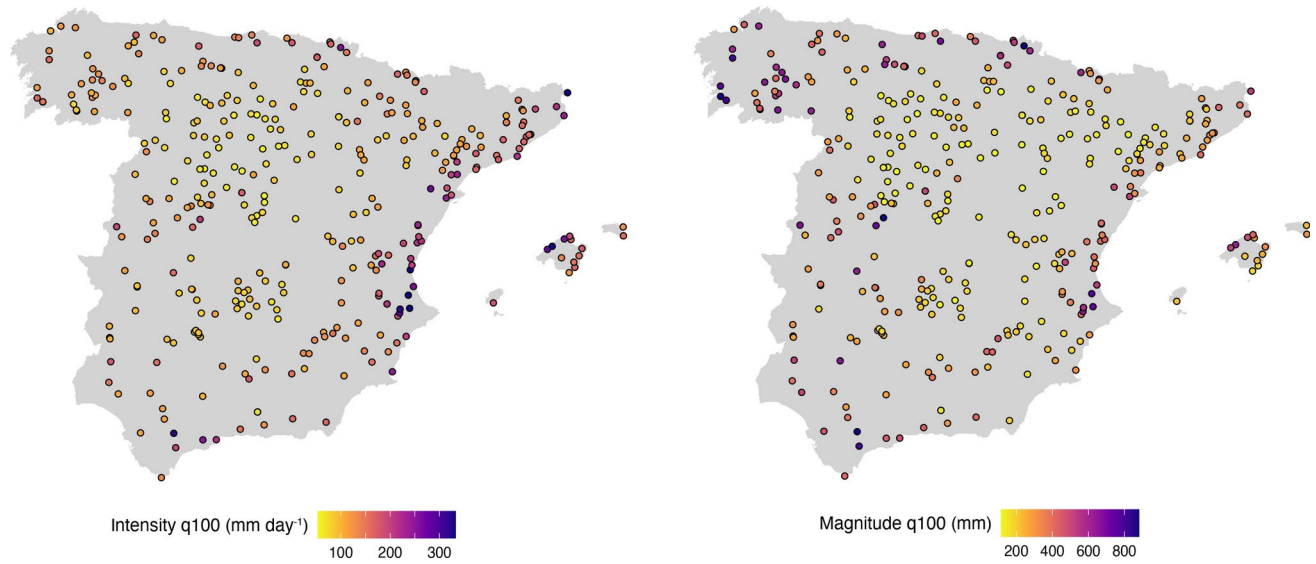

Fig. 7 Stationary model (M0): intensity and magnitude of the 100-year return period precipitation event

Table 2 Model selection: number of stations, classified according to the best-performing model (M0, M1, M2; see Table 1) as inferred from the Akaike Information Criterion (AIC) and D test

Model	AIC	D test
Event's intensity:		
M0	29	32
M1	105	18
M2	207	291
Event's magnitude:		
M0	1	1
M1	81	4
M2	259	336

3.3 Whole network analysis: effect of atmospheric indices

Results of model selection according to the AIC statistic and the D test for the whole data set are shown in Table 2. The multivariate model (M2) was the preferred one for a high number of stations (more than 60% for event's intensity, and more than 75% for magnitude). In a number of cases (30%) one of the univariate models (M1) achieved lower AIC values for the event's intensity, and only in a few cases (5%) the two non-stationary models were ruled out in favour of the simpler stationary one (M0). For the event's magnitude the non-stationary models performed better than the stationary one in all stations.

As a way In order to map the spatially varying influence of the covariates, we plotted the 100-year event conditioned to extreme values of the covariates: + and −2 for the circulation indices (NAO, WEMO and MO), and 1 and 70 (corresponding to years 1951 and 2020, respectively) for time. Figures 8 and 9 show the expected 100-year event's intensity and magnitude, respectively, for extreme values of the four covariates, according to model M2. The corresponding figures obtained with the univariate models (M1) are provided in the supplementary material (Figures A.13 and A.14). Regarding the circulation indices, the differences between extreme positive and negative phases of the indices are striking, especially in the case of the WEMO for the event's intensity and magnitude. Comparatively, the influence of time was lower than that of the circulation indices.

An alternative visualisation further highlights the influence of the different covariates in the event's intensity and magnitude (Fig. 10). The maps show the effect of each covariate on the return levels of 100-year events at each station, expressed as the ratio between extreme positive and negative values of the covariates. The color and orientation of the triangles indicate the sign of the effect, where positive means that a higher value of the covariate translates to a higher return level, and negative means an opposite relationship. The degree of influence (the ratio's magnitude) is shown by the symbol size, while the significance is indicated by a black outer triangle. The number of stations on each map classified by the sign and significance of the covariate influence is shown in Table 3.

On the remaining of this section we focus on the effect of the circulation indices, while the effect of time will be addressed in a separate sub-section. In addition to the previous maps, Fig. 11 informs about the circulation index with the strongest effect on precipitation events intensity and magnitude, as determined by the range of variation between extreme values (+2, − 2) of the indices. The maps reveal

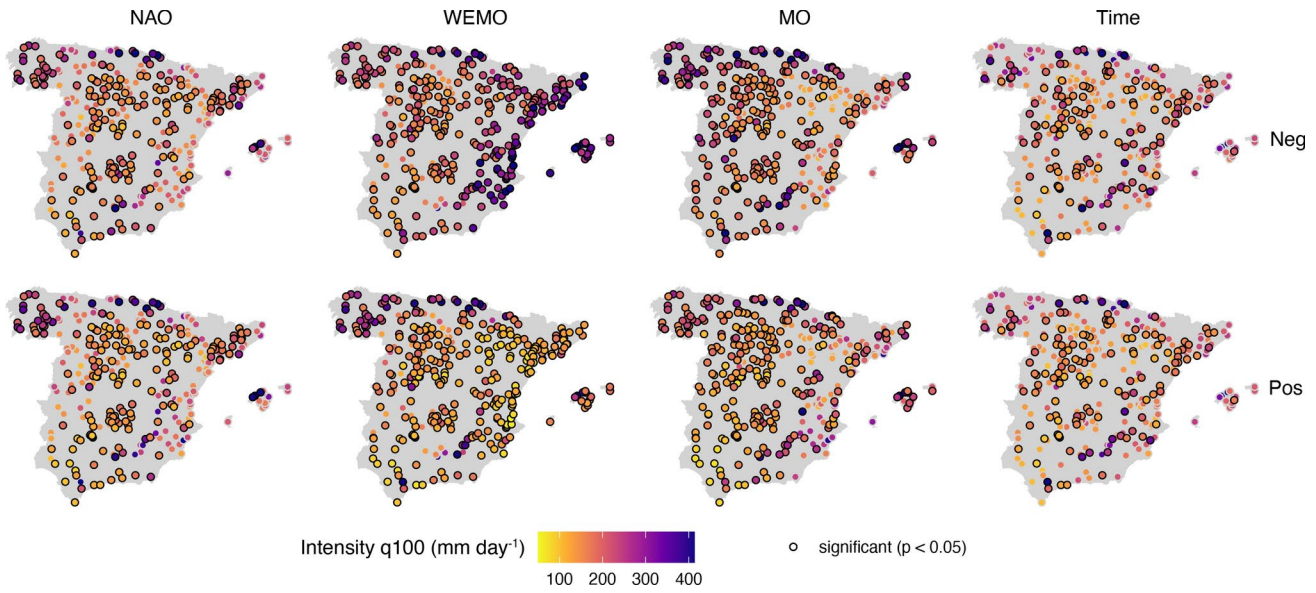

Fig. 8 Non-stationary multivariate model (M2): intensity of the 100-year return period precipitation event (q100, mm day^{-1}) for contrasting values of the covariates (Neg, top row; and Pos, bottom row): −2 and +2 for the atmospheric circulation indices (NAO, WEMO, MO), and years 1951 and 2020 for Time. Black circles denote significant relationships

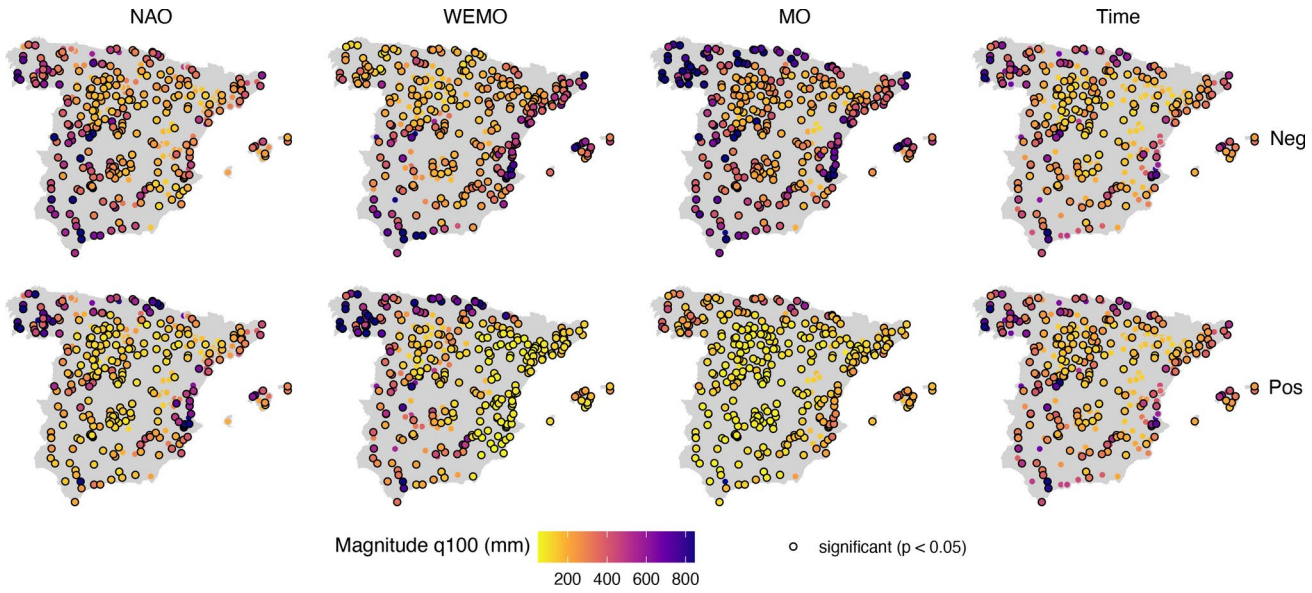

Fig. 9 Same as Fig. 8, but for event magnitude (mm)

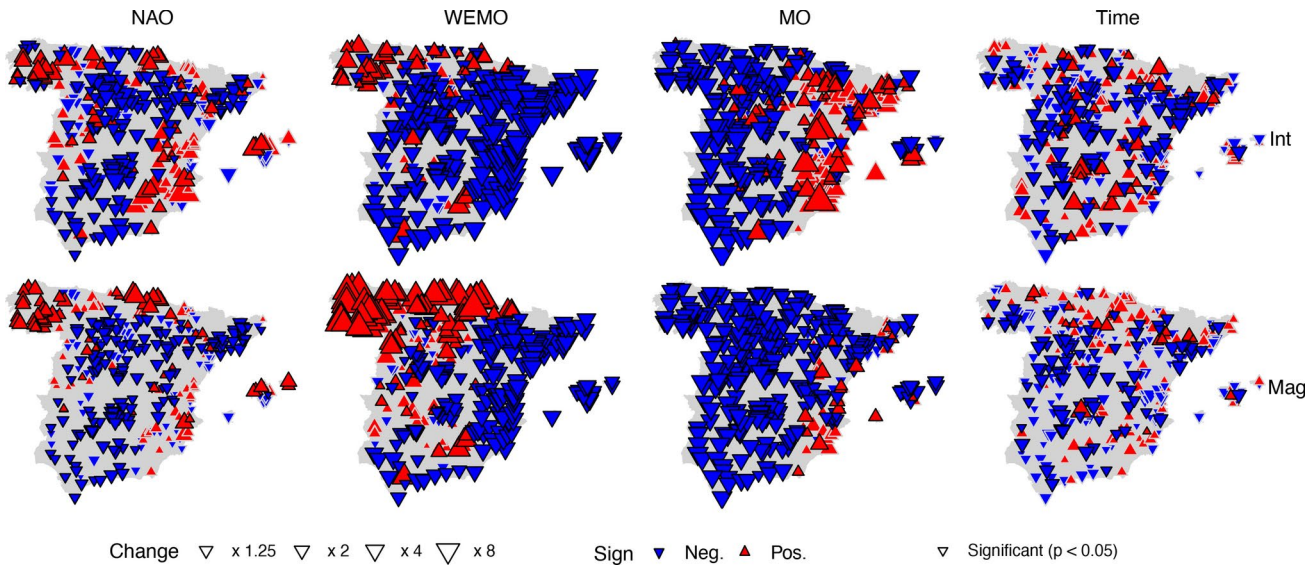

Fig. 10 Ratio between the 100-year return period event intensities (Int, top row) and magnitudes (Mag, bottom row) for contrasting values of the covariates (+2 vs. −2 for NAO, WEMO, MO; and years 70 vs. 1 for Time), for the non-stationary multivariate model (M2)

Table 3 Effect (positive or negative) and significance of the four covariates, for the multivariate non-stationary model (M2): number of stations

	NAO	WEMO	MO	Time
Event's intensity:				
Negative signif	131	255	194	102
Negative non-signif	78	24	18	110
Positive non-signif	79	15	67	99
Positive signif	53	47	62	30
Event's magnitude:				
Negative signif	156	189	284	82
Negative non-signif	70	21	16	142
Positive non-signif	60	44	25	101
Positive signif	55	87	16	16

strong influences of the three circulation indices on the extreme quantiles, with qualitatively similar patterns for the event's intensity and magnitude. The strongest effect corresponds to the WEMO, with 179 and 195 stations showing the strongest effect among the three indices for intensity and magnitude, respectively. The WEMO has a remarkable negative effect on the event's intensity and magnitude along the Mediterranean coast, extending its influence to the inner IP through the Ebro River valley. The influence of WEMO changes to positive towards the NW of the study area, especially for the event's magnitude, in agreement with the

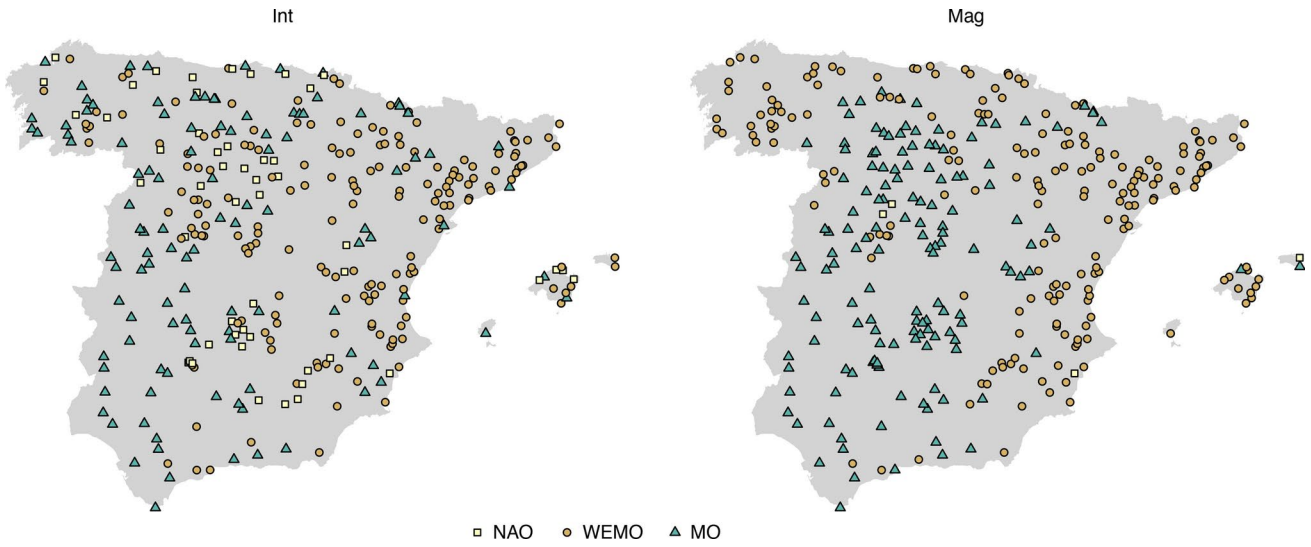

Fig. 11 Large-scale circulation patterns (NAO, WEMO, MO) that had the strongest effect on precipitation event's intensity (Int, left) and magnitude (Mag, right), for the non-stationary multivariate model (M2)

spatial fingerprints of WEMO on mean precipitation (Martin-Vide and Lopez-Bustins 2006).

The MO also has a strong and contrasting influence on the return levels, having the strongest effect among the three circulation indices in 111 and 142 stations for event's intensity and magnitude, respectively. It has a dampening effect (a negative influence) in most of the study area, and the opposite effect over the Mediterranean coast. The spatial pattern of the MO influence tends to oppose that of the WEMO, except for some regions such as the Balearic Islands where the two circulation indices have the same effect sign. This is related to the fact that the MO tends to become negative with the passage of storms in the IP that favour rains in a large part of the region. However, the Mediterranean coast is less affected by extratropical cyclones, and high precipitation events in this region are more sensitive to humid flows from the Mediterranean (related to negative WEMO).

The NAO, in comparison, has a smaller marginal effect when the other two indices are also accounted for, being the strongest effect for 51 and 4 stations for intensity and magnitude, and it also shows a less clear spatial pattern. It has a dampening effect on the return levels over the center and SW of the study area, while the stations in the NW reveal an intensification of the return values with the NAO, in particular for the event's magnitude. These results agree with previous studies reporting spatially complex responses to NAO in Spain. For example, (Queralt et al. 2009) found that the strongest and most robust increases in winter precipitation intensity are found in western and central regions of Spain during negative NAO phases, consistent with the southward shift of the storm tracks. However, positive NAO phases can be associated with increases in total precipitation and eventually intensity over northern and northwestern areas of Spain, likely due to their location in a transitional area of NAO influence.

The relative importance of the circulation indices varies seasonally and with the event attribute (intensity and magnitude), as revealed by Figures A.15 to A.18. For the event's intensity, the three atmospheric patterns have a stronger influence in winter, followed by spring and autumn, with very low significance in summer when precipitation in the IP is scarce and more linked to mesoscale convective situations than to synoptic systems. Overall, the effect of circulation indices is larger in winter and tends to decrease in spring and autumn, sometimes being also accompanied by small changes in the spatial patterns.

The spatial patterns for the event's magnitude also display some differences with respect to those of event's intensity. In this case, the influence of the circulation indices is strong in winter and spring, but less so in autumn and almost negligible in summer. For example, the NAO shows a stronger effect than in the case of the intensity, with a marked influence in the SW area in winter, extending towards central Spain. This may reflect non-linear influences on the character of the precipitation (e.g. Queralt et al. 2009).

3.4 Whole network analysis: long-term trends

Temporal trends, as shown by the time covariate, merit special attention. In general, the significance of the temporal (trend) component of the model was smaller than that of the atmospheric patterns, as seen in Table 3.

For the event's intensity, the stations with a significant temporal effect on the multivariate model amount to 38% (n = 132), with a clear predominance of negative coefficients, denoting decreasing trends in the return levels with time (n

= 102 vs 30). There is not a clear spatial pattern in the distribution of the trends, as positive and negative ones appear scattered around the study area, suggesting that these results are somehow homogenous across the area.

These results are similar for the event's magnitude, although the number of stations with a significant time effect is lower, as there were 82 stations with significant decreasing trends against 16 with significant increasing ones. Our results agree with previous studies suggesting a larger proportion of the territory displaying decreases than increases in extreme precipitation (e.g. Rodrigo 2010; Acero et al. 2011; Serrano-Notivoli et al. 2018).

It is interesting to compare between models M1 and M2 with regard to the time effect. It is noteworthy to recall that the marginal effects of covariates in M2 reflect their influence on return levels once the effect of the other covariates are also considered, while model M1 does not allow for such distinction. It is our hypothesis that model M2 would make a better job at identifying underlying long-term trends in return levels, possibly attributable to climate change, as the effect of large-scale circulation indices with their characteristic multi-decadal oscillations is accounted for. The effect and significance of the four covariates according to model M1 are provided in the supplementary material (Table A.4). As expected, the overall number of significant effects is smaller in model M2 than M1, as the dependent's variable variance is split between morea larger number of covariates. But there are also subtile shifts in the importance of the covariates, too. In the case of time, and for the event's intensity, the number of stations with significant negative trends is only slightly higher in M2 than in M1 (n = 102 vs. 98, respectively), while the number of significant positive trends is drastically reduced (n = 30 vs. 62). That is, accounting for the variability explained by circulation indices increases maintained the signal of negative trends, but reduced the overall significance of positive trends. As for the event's magnitude, the effect is a reduction of significance, both for negative (n = 82 vs. 112) and positive trends (n = 16 vs. 80). Even considering the reduction, the difference between the number of negative and positive trends is much clearly in favour of the former in M2, once large-scale atmospheric variability is accounted for.

4 Discussion

When working with extremes, trend analysis and attribution are difficult tasks due to the small samples usually available and the highly skewed nature of the variables (heavy tails), that make statistical inference extremely difficult. The non-stationary extreme value theory, however, offers a framework for addressing a number of research problems, including the study of long-term trends in extreme events and the influence of atmospheric dynamics and other covariates. Multivariate models allow to assess the marginal effects of each covariate, once the combined effect of the remaining ones has been taken into account. Since long-term trends in climatic variables are often hindered by medium-term (e.g., decadal) natural atmospheric variability, accounting for the influence of the main modes of atmospheric circulation to eliminate their possible effect on the temporal evolution of extreme events is a sensible approach.

In our study of precipitation extremes over Spain, a non-stationary multivariate model including three atmospheric circulation indices and time as covariates exhibited an overall better performance than the univariate models and the stationary ones. This model provided an unprecedented perspective of the decoupled influence of large-scale atmospheric modes and time in extreme precipitation over mainland Spain, which represents a useful tool to disentangle large internal influences operating at inter-annual time scales and long-term (externally-driven) trends in different event attributes. We found strong and significant relationships between extreme precipitation and the circulation indices, which vary spatially and seasonally, and also differ between event's intensity and magnitude.

Several previous studies offered relatable results concerning the role of different divers on extreme precipitation in Spain, which are mostly coincident with our analysis. For instance, Merino et al. (2016) showed that NAO and MO negative phases are responsible for a large part of extreme precipitation events in southwestern Spain, while WEMO explains their occurrence along the Mediterranean coast. Lopez-Bustins and Lemus-Canovas (2020) and Lopez-Bustins et al. (2020) showed that 60% of torrential precipitation events in the northern Mediterranean coast of Spain occurred under extreme negative WEMO, especially in the southwestern IP during winter and spring. Although our results are in line with these studies, we provide a more refined analysis of the spatial patterns of major circulation indices. By considering single and combined influences of these indices, our results also provide novel results. For example, the influence of MO tends to be opposite to that of WEMO, being weaker in the Mediterranean, but otherwise similar to or stronger than that of WEMO. NAO, instead, favours high precipitation events (in magnitude rather than intensity) in the southwest in winter and in the northern half of the IP in spring, with comparatively weaker effects in summer and autumn (García et al. 2018). Martinez-Artigas et al. (2021) also highlighted the role of the MO in winter and autumn precipitation, constraining the significant NAO effects to the southwestern IP in winter, as noted by other studies (e.g. Gallego et al. 2005; Rodrigo and Trigo 2007). However, our results further reveal some distinctive

influences on different event attributes, stressing the need of considering the complex multi-faceted nature of extreme events (intensity, magnitude, duration, etcetera). Overall, the effect of circulation indices tend to be larger in attributes accounting for the duration and hence the synoptic spatio-temporal scales of the event, which seems to be consistent with a synoptic control of the large-scale circulation patterns. Differently, daily maximum intensity is expected to be also influenced by local factors (e.g. topography, local circulations), less affected by circulation indices. Still, significant effects in event's intensities were also found, which can be comparable to or even larger than those in event's magnitude. This is particularly the case in regions where high precipitation is associated with short-living events, such as the areas close to the Mediterranean coast.

Regarding long-term temporal trends, we found a general decrease in intensity and magnitude of extreme events over the study period (1951-2020), with only a few locations with significant positive trends in inland areas, the northwestern plateau, the Guadalquivir River Valley, or the southeast of the study area. These patterns coincide with those by García et al. (2007), López-Moreno et al. (2010), García et al. (2018), and Serrano-Notivoli et al. (2018), who also found a dominant decrease in the intensity and frequency of high precipitation events, except along the Mediterranean fringe. However, the high frequency of weak and opposite trends, and the lack of organised patterns prevent generalised conclusions concerning national (or even regional) changes in extreme precipitation, as they may result in contradictory statements depending on the considered network.

Interestingly, the temporal patterns were much clearer in the multivariate model, which also accounted for the influence of the circulation indices. This illustrates the main advantage of this model over the more common univariate ones, as it allows to study the decoupled influence of the covariates, time included. It also opens new opportunities to improve the statistical predictability of extreme events, for instance by taking advantage of recent advances in medium-term forecasts of circulation indices (Johnson et al. 2019; Lenssen et al. 2020). These statistical models could also be exploited in combination with dynamical models (e.g. numerical weather forecasts) to improve the return period estimates in probabilistic forecasts of extreme events, given the predicted state of the covariates.

Here we explored the influence of three circulation patterns affecting precipitation over the IP, but NSEVT models can be extended to other observational covariates and additional meteorological covariates (e.g. vorticity, convection indices, wind shear) in observational-derived products (reanalysis). In the case of the IP, for instance, sea surface temperature anomalies over the western Mediterranean are a plausible candidate that would be worth exploring, as suggested by Pastor et al. (2001) and Rigo et al. (2019).

NSEVT models are also frequently employed in extreme event attribution in order to infer anthropogenic-induced changes in the event's intensity or probability of occurrence (National Academies of Sciences et al. 2016; Stott et al. 2016; Naveau et al. 2020; Philip et al. 2020). These changes are often quantified by comparing two frequency-magnitude curves, one for present-day conditions and other for a hypothetical naturalised world without human influences (e.g. pre-industrial climate). When applied to observations, a non-stationary model is constructed by taking global mean temperature as a covariate (or other covariate with strong anthropogenic influences), which allows establishing linkages of the event to anthropogenic factors (Naveau et al. 2020; Philip et al. 2020). As the short length of observations impede estimating the model parameters for a preindustrial climate, the non-stationary model relies on past estimates of the threshold inferred from a linear regression with the covariate. This approach assumes a linear dependence with the covariate and ignores changes in variability, which can be important for extremes. Our model could be adapted for attribution (e.g. by replacing time with global mean temperature) to estimate how recent extreme events could have been in a past world with reduced anthropogenic influences (e.g. the 1950 s). While this does not account for the entire climate change signal, it avoids assumptions on linearity and time-invariant model parameters.

The use of additional dynamical covariates could be employed to perform conditional attribution, i.e. restricted to conditions that were observed at the time of the event, such as sea surface temperature or the atmospheric circulation (National Academies of Sciences et al. 2016; Stott et al. 2016; Barriopedro et al. 2020). Previous studies have shown that conditioning on relevant drivers of the event can avoid false negative results in attribution, particularly when these covariates show small or uncertain responses to climate change, as it is the case of circulation patterns (Shepherd 2016). Ignoring the uncertain changes in dynamical aspects may yield to overstatements in attribution (i.e. false positives), but it also allows addressing robust (thermodynamical) influences of climate change on the event.

5 Conclusion

We performed a non-stationary peaks-over-threshold analysis of extreme precipitation events in Spain over a period of 70 years (1951-2020) by using an observational network of 341 quality-checked and infilled weather stations. As independent variables (covariates) we considered time and three major circulation patterns with known influences in

precipitation over the Iberian Peninsula, namely the North Atlantic Oscillation, Mediterranean Oscillation and Western Mediterranean Oscillation. Univariate and multivariate non-stationary models conditioning the magnitude / frequency relationship on these covariates were constructed, and compared to a stationary model in order to determine the best-fitting model across the observational network. The approach was applied to two main attributes of extreme precipitation events (daily peak intensity and accumulated precipitation magnitude), defined on annual and seasonal scales. The main conclusions can be summarised as follows:

- Circulation indices have a prominent role in shaping the extreme value curves, with coherent regional patterns and substantial seasonal variation (stronger signal in winter and spring).
- The Western Mediterranean Oscillation (WEMO) exerts its largest influences over the Mediterranean area, while the North Atlantic Oscillation (NAO) is strongest over the SW, and the Mediterranean Oscillation (MO) playing a secondary but complementary role in precipitation event's intensity and magnitude.
- There was no strong and conclusive proof of temporal trends in event's intensity or magnitude, although the number of series exhibiting a significant negative trend (that is, towards lower extreme events) was higher than the positive ones, especially for the event's intensity.
- Unlike univariate approaches for trend detection, multivariate models can increase the signal-to-noise ratio by removing confounding influences of the climate's internal modes of variability.

These results illustrate the advantages of including relevant atmospheric covariates in extreme value analysis, as they allow to parametrically explore the relationship between these covariates and extreme events. In the case of time as a covariate, including other relevant covariates allows to assess long-term temporal trends without the interference of inter-annual to multi-decadal variations in the covariates, which may hamper the detection.

These results are promising for a variety of applications, including, but not restricted to, the statistical downscaling of GCM / RCM output, the development of extreme precipitation warning systems, or extreme event's attribution to climate change.

Supplementary Information The online version contains supplementary material available at https://doi.org/10.1007/s00477-025-02961-x.

Acknowledgements This research work has been funded by the Spanish National Research Agency (MCIN/AEI) through project PID2020-116860RB-C22 and R.S.-N. personal grant RYC2021-034330-I, by the European Commission - NextGenerationEU (Regulation EU 2020/2094) through CSIC's Interdisciplinary Thematic Platform "Clima (PTI Clima) / Development of Operational Climate Services", and by Aragón Government through grant E02-20R.

Author contributions Santiago Beguería: Conceptualization, Methodology, Software, Formal Analysis, Writing - Original Draft, Funding acquisition. Miquel Tomas-Burguera: Conceptualization, Validation, Writing - Review & Editing. Roberto Serrano-Notivoli: Conceptualization, Validation, Writing - Review & Editing. David Barriopedro: Conceptualization, Writing - Review & Editing. Sergio M. Vicente-Serrano: Conceptualization, Writing - Review & Editing.

Funding Open Access funding provided thanks to the CRUE-CSIC agreement with Springer Nature.

Data availability No datasets were generated or analysed during the current study.

Declarations

Conflict of interest The authors declare no conflict of interest.

References

Abaurrea J, Asín J, Cebrián A, Centelles A (2007) Modeling and forecasting extreme hot events in the central ebro valley, a continental-mediterranean area. Global Planet Change 57(1):43–58

Acero FJ, García JA, Gallego MC (2011) Peaks-over-threshold study of trends in extreme rainfall over the Iberian peninsula. J Clim 24(4):1089–1105

Agilan V, Umamahesh N (2015) Detection and attribution of non-stationarity in intensity and frequency of daily and 4-h extreme rainfall of hyderabad, india. J Hydrol 530:677–697. https://doi.org/10.1016/j.jhydrol.2015.10.028

Agilan V, Umamahesh N (2016) Is the covariate based non-stationary rainfall idf curve capable of encompassing future rainfall changes? J Hydrol 541:1441–1455. https://doi.org/10.1016/j.jhydrol.2016.08.052

Agilan V, Umamahesh N (2017) What are the best covariates for developing non-stationary rainfall intensity-duration-frequency relationship? Adv Water Resour 101:11–22

Balkema AA, De Haan L (1974) Residual life time at great age. Ann Probab 2(5):792–804

Barriopedro D, Sousa P, Trigo R, García-Herrera R, Ramos A (2020) The exceptional iberian heatwave of summer 2018. Bull Am Meteor Soc 101(1):S29–S34

Beguería S (2005) Uncertainties in partial duration series modelling of extremes related to the choice of the threshold value. J Hydrol 303(1):215–230

Beguería S (2023) Gap-filling of daily time series of climatic data, version 1.0.0. https://github.com/sbegueria/gap_filling

Beguería S, Angulo-Martínez M, Vicente-Serrano SM, López-Moreno JI, El-Kenawy A (2011) Assessing trends in extreme precipitation events intensity and magnitude using non-stationary peaks-over-threshold analysis: a case study in northeast spain from 1930 to 2006. Int J Climatol 31(14):2102–2114

Beguería S, Tomas-Burguera M, Serrano-Notivoli R, Peña-Angulo D, Vicente-Serrano SM, González-Hidalgo JC (2019) Gap filling of monthly temperature data and its effect on climatic variability and trends. J Clim 32(22):7797–7821

Casanueva A, Rodríguez-Puebla C, Frías M, González-Reviriego N (2014) Variability of extreme precipitation over Europe and its relationships with teleconnection patterns. Hydrol Earth Syst Sci 18(2):709–725

Cheng L, Aghakouchak A (2014) Nonstationary precipitation intensity-duration-frequency curves for infrastructure design in a changing climate. Sci Rep 4:7093

Coles S, Bawa J, Trenner L, Dorazio P (2001) An introduction to statistical modeling of extreme values, vol 208. Springer

Conte M, Giuffrida A, Tedesco S (1989) The mediterranean oscillation: impact on precipitation and hydrology in italy

Fisher LRA, Tippett LHC (1928) Limiting forms of the frequency distribution of the largest and smallest member of a sample. Proc Cambridge Philos Trans 24(2):180

Fowler HJ, Kilsby CG (2003) A regional frequency analysis of united kingdom extreme rainfall from 1961 to 2000. Int J Climatol 23(11):1313–1334. https://doi.org/10.1002/joc.943

Fréchet M (1927) Sur la loi de probabilité de l'écart maximum. Annales de la Société Polonaise de Mathématique 6(1):93

Friederichs P (2010) Statistical downscaling of extreme precipitation events using extreme value theory. Extremes 13(2):109–132

Gallego M, García J, Vaquero J (2005) The nao signal in daily rainfall series over the Iberian peninsula. Climate Res 29:103–109. https://doi.org/10.3354/cr029103

Gallego M, Trigo R, Vaquero J, Brunet M, García J, Sigró J, Valente M (2011) Trends in frequency indices of daily precipitation over the Iberian peninsula during the last century. J Geophys Res: Atmospheres. https://doi.org/10.1029/2010JD014255

Ganguli P, Coulibaly P (2017) Does nonstationarity in rainfall requires nonstationary intensity-duration-frequency curves? Hydrol Earth Syst Sci 21:6461–6483

Gao M, Mo D, Wu X (2016) Nonstationary modeling of extreme precipitation in China. Atmos Res 182:1–9. https://doi.org/10.1016/j.atmosres.2016.07.014

García J, Martín J, Naranjo L, Acero F (2018) A bayesian hierarchical spatio-temporal model for extreme rainfall in extremadura (spain). Hydrol Sci J 63(6):878–894

García JA, Gallego MC, Serrano A, Vaquero JM (2007) Trends in block-seasonal extreme rainfall over the Iberian peninsula in the second half of the twentieth century. J Clim 20(1):113–130

García-Herrera R, Hernández E, Paredes D, Barriopedro D, Correoso JF, Prieto L (2005) A mascotte-based characterization of mcss over spain, 2000–2002. Atmos Res 73(3–4):261–282

Gnedenko B (1943) Sur la distribution limite du terme maximum d'une serie aleatoire. Ann Math 44(3):423

Goswami P, Peterson TJ, Mondal A, Rüdiger C (2022) Non-stationary influences of large-scale climate drivers on low flow extremes in southeast Australia. Water Resour Res 58(7):e2021WR031508. https://doi.org/10.1029/2021WR031508

Gumbel EJ (1958) Statistics of Extremes. Columbia University Press, New York

Hall P, Tajvidi N (2000) Nonparametric analysis of temporal trend when fitting parametric models to extreme-value data. Statistical Science pp 153–167

Hamdi Y, Charron C, Ouarda TBMJ (2021) A non-stationary heat spell frequency, intensity, and duration model for France, integrating teleconnection patterns and climate change. Atmosphere. https://doi.org/10.3390/atmos12111387

...Hersbach H, Bell B, Berrisford P, Hirahara S, Horányi A, Muñoz-Sabater J, Nicolas J, Peubey C, Radu R, Schepers D, Simmons A, Soci C, Abdalla S, Abellan X, Balsamo G, Bechtold P, Biavati G, Bidlot J, Bonavita M, De Chiara G, Dahlgren P, Dee D, Diamantakis M, Dragani R, Flemming J, Forbes R, Fuentes M, Geer A, Haimberger L, Healy S, Hogan RJ, Hólm E, Janisková M, Keeley S, Laloyaux P, Lopez P, Lupu C, Radnoti G, de Rosnay P, Rozum I, Vamborg F, Villaume S, Thépaut JN (2020) The era5 global reanalysis. Q J R Meteorol Soc 146(730):1999–2049. https://doi.org/10.1002/qj.3803

Heffernan Janet E, EG, Stephenson Alec G (2018) ismev: An Introduction to Statistical Modeling of Extreme Values (R package version 1.42). https://CRAN.R-project.org/package=ismev

Johnson SJ, Stockdale TN, Ferranti L, Balmaseda MA, Molteni F, Magnusson L, Tietsche S, Decremer D, Weisheimer A, Balsamo G, Keeley SPE, Mogensen K, Zuo H, Monge-Sanz BM (2019) Seas5: the new ecmwf seasonal forecast system. Geosci Model Dev 12(3):1087–1117. https://doi.org/10.5194/gmd-12-1087-2019

Kallache M, Vrac M, Naveau P, Michelangeli PA (2011) Nonstationary probabilistic downscaling of extreme precipitation. J Geophys Res: Atmospheres. https://doi.org/10.1029/2010JD014892

Koenker R (2022) quantreg: Quantile Regression (R package version 5.94). https://CRAN.R-project.org/package=quantreg

Kyselỳ J, Picek J, Beranová R (2010) Estimating extremes in climate change simulations using the peaks-over-threshold method with a non-stationary threshold. Global Planet Change 72(1–2):55–68

Laurent C, Parey S (2007) Estimation of 100-year-return-period temperatures in France in a non-stationary climate: Results from observations and ipcc scenarios. Global Planet Change 57(1):177–188

Leadbetter MR (1991) On a basis for 'peaks over threshold'modeling. Stat Prob Lett 12(4):357–362

Lee O, Sim I, Kim S (2019) Application of the non-stationary peak-over-threshold methods for deriving rainfall extremes from temperature projections. J Hydrol. https://doi.org/10.1016/j.jhydrol.2019.124318

Lenssen NJL, Goddard L, Mason S (2020) Seasonal forecast skill of enso teleconnection maps. Weather Forecasting 35(6):2387–2406. https://doi.org/10.1175/WAF-D-19-0235.1

Li Y, Cai W, Campbell E (2005) Statistical modeling of extreme rainfall in southwest western Australia. J Clim 18(6):852–863

Lopez-Bustins JA, Lemus-Canovas M (2020) The influence of the western Mediterranean oscillation upon the spatio-temporal variability of precipitation over catalonia (northeastern of the Iberian peninsula). Atmos Res 236:104819. https://doi.org/10.1016/j.atmosres.2019.104819

Lopez-Bustins JA, Arbiol-Roca L, Martin-Vide J, Barrera-Escoda A, Prohom M (2020) Intra-annual variability of the western Mediterranean oscillation (wemo) and occurrence of extreme torrential precipitation in catalonia (ne Iberia). Nat Hazard 20(9):2483–2501

López-Moreno J, Vicente-Serrano S, Angulo-Martínez M, Beguería S, Kenawy A (2010) Trends in daily precipitation on the north-eastern Iberian peninsula, 1955–2006. Int J Climatol 30(7):1026–1041. https://doi.org/10.1002/joc.1945

Maraun D, Rust HW, Osborn TJ (2010) Synoptic airflow and uk daily precipitation extremes. Extremes 13(2):133–153

Martin-Vide J, Lopez-Bustins JA (2006) The western Mediterranean oscillation and rainfall in the Iberian peninsula. Int J Climatol 26(11):1455–1475

Martinez-Artigas J, Lemus-Cánovas M, López-Bustins J (2021) Precipitation in peninsular Spain: Influence of teleconnection indices and spatial regionalisation. Int J Climatol 41(S1):E1320–E1335. https://doi.org/10.1002/joc.6770

Méndez FJ, Menéndez M, Luceño A, Losada IJ (2006) Estimation of the long-term variability of extreme significant wave height using a time-dependent peak over threshold (pot) model. Journal of Geophysical Research: Oceans 111(C7)

Merino A, Fernández-Vaquero M, López L, Fernández-González S, Hermida L, Sánchez J, García-Ortega E, Gascón E (2016) Large-scale patterns of daily precipitation extremes on the Iberian peninsula. Int J Climatol 36(11):3873–3891. https://doi.org/10.1002/joc.4601

Mondal A, Mujumdar P (2015) Modeling non-stationarity in intensity, duration and frequency of extreme rainfall over India. J Hydrol 521:217–231. https://doi.org/10.1016/j.jhydrol.2014.11.071

Nasri B, Tramblay Y, El Adlouni S, Hertig E, Ouarda TB (2016) Atmospheric predictors for annual maximum precipitation in North Africa. J Appl Meteorol Climatol 55(4):1063–1076

Naveau P, Hannart A, Ribes A (2020) Statistical methods for extreme event attribution in climate science. Ann Rev Stat Appl 7:89–110

Nogaj M, Yiou P, Parey S, Malek F, Naveau P (2006) Amplitude and frequency of temperature extremes over the North Atlantic region. Geophys Res Lett. https://doi.org/10.1029/2005GL024251

O'Brien NL, Burn DH (2018) A nonstationary peaks-over-threshold approach for modelling daily precipitation with covariate-dependent thresholds. Can Water Resour J /Revue canadienne des ressources hydriques 43(3):281–304

Ouarda TB, Yousef LA, Charron C (2019) Non-stationary intensity-duration-frequency curves integrating information concerning teleconnections and climate change. Int J Climatol 39(4):2306–2323

Palutikof J (2003) Analysis of mediterranean climate data: measured and modelled. In: Mediterranean Climate, Springer, pp 125–132

Parey S, Malek F, Laurent C, Dacunha-Castelle D (2007) Trends and climate evolution: statistical approach for very high temperatures in France. Clim Change 81(3–4):331–352

Pastor F, Estrela MJ, Peñarrocha D, Millán MM (2001) Torrential rains on the spanish mediterranean coast: modeling the effects of the sea surface temperature. J Appl Meteorol 40(7):1180–1195

Pérez-Zanón N, Casas-Castillo MC, Peña JC, Aran M, Rodríguez-Solà R, Redaño A, Solé G (2018) Analysis of synoptic patterns in relationship with severe rainfall events in the Ebre observatory (catalonia). Acta Geophys 66:405–414

Philip S, Kew S, van Oldenborgh G, Otto F, Vautard R, van der Wiel K, King A, Lott F, Arrighi J, Singh R et al (2020) A protocol for probabilistic extreme event attribution analyses. Adv Stat Climatol Meteorol Oceanogr 6:177–203

Pickands III J (1975) Statistical inference using extreme order statistics. the Annals of Statistics pp 119–131

Queralt S, Hernández E, Barriopedro D, Gallego D, Ribera P, Casanova C (2009) North atlantic oscillation influence and weather types associated with winter total and extreme precipitation events in spain. Atmos Res 94(4):675–683

Ramis C, Homar V, Amengual A, Romero R, Alonso S (2013) Daily precipitation records over mainland Spain and the Baleadric islands. Nat Hazard 13(10):2483–2491

Rigo T, Berenguer M, del Carmen Llasat M (2019) An improved analysis of mesoscale convective systems in the western Mediterranean using weather radar. Atmos Res 227:147–156. https://doi.org/10.1016/j.atmosres.2019.05.001

Ríos-Cornejo D, Penas Á, Álvarez-Esteban R, del Río S (2015) Links between teleconnection patterns and precipitation in Spain. Atmos Res 156:14–28

Rodrigo F (2010) Changes in the probability of extreme daily precipitation observed from 1951 to 2002 in the Iberian peninsula. Int J Climatol 30(10):1512–1525

Rodrigo F, Trigo R (2007) Trends in daily rainfall in the Iberian peninsula from 1951 to 2002. Int J Climatol 27(4):513–529. https://doi.org/10.1002/joc.1409

Rodríguez-Puebla C, Encinas A, Jy Sáenz (2001) Winter precipitation over the Iberian peninsula and its relationship to circulation indices. Hydrol Earth Syst Sci 5(2):233–244

Roth M, Jongbloed G, Buishand A (2019) Monotone trends in the distribution of climate extremes. Theoret Appl Climatol 136(3–4):1175–1184

Sarhadi A, Ausín MC, Wiper MP (2016) A new time-varying concept of risk in a changing climate. Sci Rep 6:35755

National Academies of Sciences E, Medicine, et al (2016) Attribution of extreme weather events in the context of climate change. National Academies Press

Serrano-Notivoli R, Beguería S, Saz M, de Luis M (2018) Recent trends reveal decreasing intensity of daily precipitation in Spain. Int J Climatol 38(11):4211–4224. https://doi.org/10.1002/joc.5562

Service CCC (2017) Era5: Fifth generation of ecmwf atmospheric reanalyses of the global climate. https://cds.climate.copernicus.eu/cdsapp

Shepherd TG (2016) A common framework for approaches to extreme event attribution. Curr Climate Change Rep 2:28–38

Silva AT, Naghettini M, Portela MM (2016) On some aspects of peaks-over-threshold modeling of floods under nonstationarity using climate covariates. Stoch Env Res Risk Assess 30(1):207–224

Smith RL (1989) Extreme value analysis of environmental time series: an application to trend detection in ground-level ozone. Stat Sci 4(4):367–393

Smith RL (1999) Trends in rainfall extremes

Stephenson DB, Wanner H, Brönnimann S, Luterbacher J (2003) The History of Scientific Research on the North Atlantic Oscillation, American Geophysical Union (AGU), pp 37–50. https://doi.org/10.1029/134GM02

Stott PA, Christidis N, Otto FE, Sun Y, Vanderlinden JP, van Oldenborgh GJ, Vautard R, von Storch H, Walton P, Yiou P et al (2016) Attribution of extreme weather and climate-related events. Wiley Interdisciplinary Rev: Climate Change 7(1):23–41

Thiombiano AN, El Adlouni S, St-Hilaire A, Ouarda TB, El-Jabi N (2017) Nonstationary frequency analysis of extreme daily precipitation amounts in southeastern Canada using a peaks-over-threshold approach. Theoret Appl Climatol 129(1–2):413–426

Tramblay Y, Neppel L, Carreau J, Sanchez-Gomez E (2012) Extreme value modelling of daily areal rainfall over Mediterranean catchments in a changing climate. Hydrol Process 26(25):3934–3944. https://doi.org/10.1002/hyp.8417

Tramblay Y, Neppel L, Carreau J, Najib K (2013) Non-stationary frequency analysis of heavy rainfall events in southern France. Hydrol Sci J 58(2):280–294. https://doi.org/10.1080/02626667.2012.754988

Trigo RM, Osborn TJ, Corte-Real JM (2002) The North Atlantic oscillation influence on Europe: climate impacts and associated physical mechanisms. Climate Res 20(1):9–17

Tu K, Yan Z (2021) Non-stationary climate changes in summer high-temperature extremes in shanghai since the late 19th century. Int J Climatol 41(S1):E718–E733. https://doi.org/10.1002/joc.6721

Vicente-Serrano SM, López-Moreno JI (2008) Nonstationary influence of the north atlantic oscillation on european precipitation. Journal of Geophysical Research: Atmospheres 113(D20)

Vicente-Serrano SM, Beguería S, López-Moreno JI, El Kenawy AM, Angulo-Martínez M (2009) Daily atmospheric circulation events and extreme precipitation risk in northeast spain: Role of the north atlantic oscillation, the western mediterranean oscillation, and the mediterranean oscillation. Journal of Geophysical Research: Atmospheres 114(D8)

Weibull W (1951) A statistical distribution function of wide applicability. J Appl Mech- Trans ASME 18(3):293–297

Yilmaz A, Hossain I, Perera B (2014) Effect of climate change and variability on extreme rainfall intensity–frequency–duration relationships: a case study of melbourne. Hydrology & Earth System Sciences 18(10)

Yilmaz A, Imteaz M, Perera B (2017) Investigation of non-stationarity of extreme rainfalls and spatial variability of rainfall intensity-frequency-duration relationships: a case study of victoria, australia. Int J Climatol 37(1):430–442

Yilmaz AG, Perera BJC (2014) Extreme rainfall nonstationarity investigation and intensity-frequency-duration relationship. J Hydrol Eng 19(6):1160–1172. https://doi.org/10.1061/(ASCE)HE.1943-5584.0000878

Yiou P, Ribereau P, Naveau P, Nogaj M, Brázdil R (2006) Statistical analysis of floods in bohemia (czech republic) since 1825. Hydrol Sci J 51(5):930–945